water

MDPI

Article

Nitrate Source and Transformation in Groundwater under Urban and Agricultural Arid Environment in the Southeastern Nile Delta, Egypt

Alaa M. Kasem [1,2,3], Zhifang Xu [1,2,4,*], Hao Jiang [5], Wenjing Liu [1,2,4], Jiangyi Zhang [1,2,4] and Ahmed M. Nosair [6]

1 Key Laboratory of Cenozoic Geology and Environment, Institute of Geology and Geophysics, Chinese Academy of Sciences, Beijing 100029, China; alaa.kasem@cu.edu.eg (A.M.K.); liuwenjing@mail.iggcas.ac.cn (W.L.); zhangjiangyi@mail.iggcas.ac.cn (J.Z.)
2 University of Chinese Academy of Sciences, Beijing 100049, China
3 Department of Natural Resources, Faculty of African Postgraduate Studies, Cairo University, Giza 12613, Egypt
4 CAS Center for Excellence in Life and Paleoenvironment, Beijing 100044, China
5 Key Laboratory of Aquatic Botany and Watershed Ecology, Wuhan Botanical Garden, Chinese Academy of Sciences, Wuhan 430074, China; jianghao@wbgcas.cn
6 Environmental Geophysics Lab (ZEGL), Geology Department, Faculty of Science, Zagazig University, Zagazig 44519, Egypt; ahmed_nosair@zu.edu.eg
* Correspondence: zfxu@mail.iggcas.ac.cn; Tel.: +86-010-82998289; Fax: +86-010-62010846

Abstract: With the intensification of human activities, nitrate pollutants in groundwater are receiving increasing attention worldwide. Especially in the arid Nile Delta of Egypt, groundwater is one of the most valuable water resources in the region. Identifying the source of nitrate in groundwater with strong human disturbances is important to effective water resource management. This paper examined the stable isotopes ($\delta^{15}N/\delta^{18}O\text{-}NO_3$ and $\delta^{2}H/\delta^{18}O\text{-}H_2O$) and the hydrogeochemical parameters of the shallow groundwaters in the arid southeast of the Nile Delta to assess the potential sources and transformation processes of nitrate under severe urban and agricultural activities. The results revealed that the groundwaters were recharged by the Nile River. Meanwhile, the infiltration of irrigation water occurred in the west, while the mixing with the deep groundwater occurred in the east regions of the study area. The TDS, SO_4^{2-}, NO_3^-, and Mn^{2+} concentrations of groundwaters (n = 55) exceeded the WHO permissible limit with 34.6%, 23.6%, 23.6%, and 65.5%, respectively. The NO_3^- concentrations in the shallow groundwaters ranged from 0.42 mg/L to 652 mg/L, and the higher levels were observed in the middle region of the study area where the unconfined condition prevailed. It extended to the deep groundwater and eastward of the study area in the groundwater flow direction. The $\delta^{15}N\text{-}NO_3$ and $\delta^{18}O\text{-}NO_3$ values suggested that the groundwater NO_3^- in the west and east regions of semi-confined condition were largely from the nitrification of soil organic nitrogen (SON) and chemical fertilizer (CF). In contrast, wastewater input (e.g., domestic sewage and unlined drains) and prevalent denitrification were identified in the middle region. The denitrification might be tightly coupled with the biogeochemical cycling of manganese. This study provides the first report on the groundwater NO_3^- dynamics in the Nile Delta, which generated valuable clues for effective water resource management in the arid region.

Keywords: nitrate pollution; dual nitrate isotopes; water isotopes; the Nile Delta

check for updates

Citation: Kasem, A.M.; Xu, Z.; Jiang, H.; Liu, W.; Zhang, J.; Nosair, A.M. Nitrate Source and Transformation in Groundwater under Urban and Agricultural Arid Environment in the Southeastern Nile Delta, Egypt. *Water* **2024**, *16*, 22. https://doi.org/10.3390/w16010022

Academic Editor: Alexander Yakirevich

Received: 21 November 2023
Revised: 15 December 2023
Accepted: 18 December 2023
Published: 20 December 2023

1. Introduction

Groundwater nitrate (NO_3^-) pollution resulting from human activities is a pressing global concern [1,2]. Particularly, regions with high population density and intensive land use face increased vulnerability to this contamination [3–8]. This issue is prevalent in arid and semi-arid areas where water scarcity is already a significant challenge [9–11].

High NO_3^- levels in groundwater cause ecological issues such as eutrophication of nearby surface water and hypoxia [1,12–18]. Furthermore, NO_3^- in drinking water has been associated with health risks such as methemoglobinemia and cancer [19–22]. In response to the prevailing health concerns associated with NO_3^- contamination, the World Health Organization (WHO) has set a maximum threshold of 50 mg/L for drinking water [23].

To effectively manage NO_3^- pollution in groundwaters, a comprehensive understanding of its sources and transformation processes is necessary. While NO_3^- stems from various sources, including agricultural practices, wastewater, organic matter in the soil, atmospheric nitrogen deposition [24–26], and complex transformation processes such as denitrification and nitrification [27–29] make it more difficult to determine the exact source of nitrate. The use of isotopic tracer techniques, particularly dual NO_3^- stable isotopes, has been widely employed in various areas to investigate NO_3^- sources and transformations based on the distinct isotopic compositions of NO_3^- sources and the predictable isotopic fractionations [22,30–38]. For instance, studies have utilized the dual NO_3^- isotopes to explore the relationship between NO_3^- contamination in groundwaters and agricultural practices [39] and urban activities [30].

Despite the widespread use of this approach, uncertainties can arise when attempting to identify NO_3^- sources [40–42]. First, isotopic compositions of NO_3^- arising from various sources can exhibit some degree of overlap [38]. Second, the isotope fractionation process may obscure the initial isotopic compositions [38]. Therefore, other isotopes (e.g., $\delta^2H/\delta^{18}O$-H_2O and $\delta^{11}B$), water chemistry (e.g., Cl^- and SO_4^{2-}), and hydrogeochemical parameters were jointly applied to enhance the accuracy of NO_3^- source identification [22,43–48]. The integration of these additional data sets is expected to provide valuable and definitive insights into both water and NO_3^- cycling dynamics.

In the arid Nile Delta, the groundwater is a valuable resource because people rely on it for different purposes. The growing population, rapid urbanization, and increased usage of chemical fertilizers have led to severe NO_3^- pollution in the groundwaters. The authors of [49] highlighted significant urban expansion in the Nile Delta region from 1987 to 2015. It is presumed that this expansion has led to an increase in the discharge of untreated wastewater into water bodies. Furthermore, the two main wastewater unlined drains (Belbies and Kalyobiya) cross the study areas. These pollutants will inevitably infiltrate into the groundwater. High NO_3^- levels in the groundwaters have been reported (210 mg/L); however, the sources of pollution have not yet been identified, and the driving mechanisms still remain to be studied. There has been a lack of isotopic studies on NO_3^- pollution in the groundwaters in this region [50,51]. This seriously hinders the implementation of groundwater nitrate pollution prevention and control work in the region.

Located at the eastern fringe of the Nile Delta, the studied area is characterized with unlined drainage channels crisscrossing, a wide distribution of illegal shallow wells, and the expansion of urban areas, which further deteriorate the problem of groundwater pollution. In this study, for the first time, we use an integrating approach of a multiple isotope tracer ($\delta^{15}N/\delta^{18}O$-$NO_3$ and $\delta^2H/\delta^{18}O$-H_2O) combined with hydrogeochemical parameters to identify the sources of NO_3^- contamination and its transportation and transformation processes in the shallow groundwater of this area. The results are expected to provide insights to the effective management of the water resources in the arid region with intense human disturbance.

2. Materials and Methods

2.1. Study Area

The study area is located in the southeastern Nile Delta, a natural extension of the Nile Delta floodplain stretching toward the east. It extends between longitudes 31°3′22.42″–31°40′25.4″ E and latitudes 31°14′4.87″–30°37′16.87″ N and covers an area of approximately 2050 km^2 (Figure 1a). The study area had a population of roughly 12 million people, and the population density was calculated to be 5800 individuals/km^2 [52]. The land use is dominated by the interrelation of rural–urban and agricultural lands (Figure S2). The

cultivation in the area primarily relies on Nile River water and groundwater for irrigation as a water source. The climate is arid and rainless in summer (May to September), with temperatures ranging from 30 to 40 °C, while the winter season (November to February) is relatively mild, with precipitation ranging from 10 to 20 mm/year and temperatures ranging from 10 to 20 °C. The study area is typically characterized by its flat plains forming the Delta landscape, gently sloping toward the north–northeast and east. It exhibits low elevation and is surrounded by a moderately elevated plateau to the south and southeast (Figure 1b).

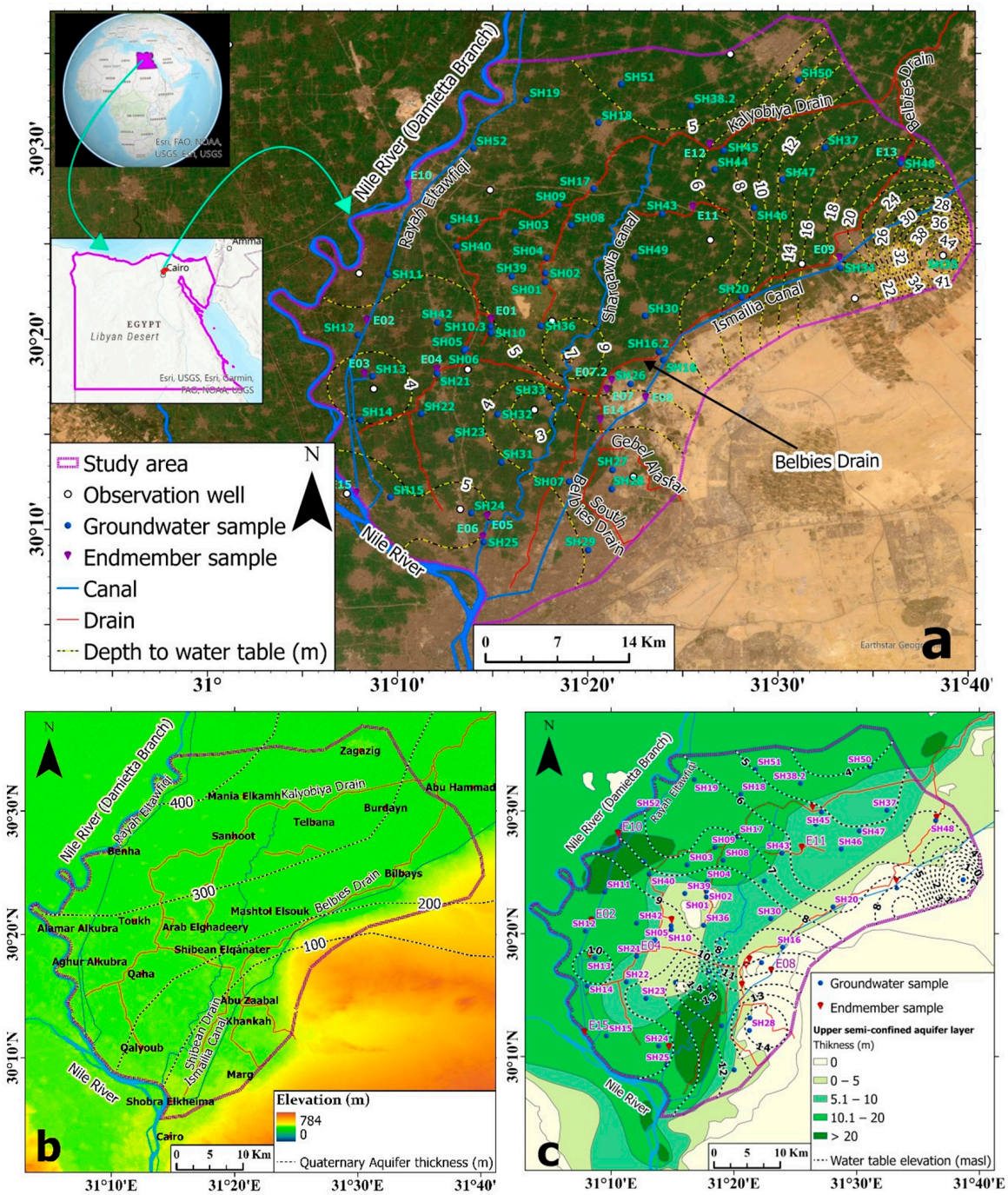

Figure 1. Maps of the study area and the sampling sites. (**a**) Landsat 8 and depth to the water table; (**b**) digital elevation model (DEM) and aquifer thickness; and (**c**) thickness of the upper semi-confined aquifer layer (modified from [53]) and hydraulic head.

The Quaternary aquifer is semi-confined and consists of two main units, the semi-pervious upper Holocene silt, sand, and silty clay unit (upper Holocene layer) (Figures S1 and S3), with thickness ranging from 0 to 20 m (Figure 1c) [53]. It is underlain by unconsolidated Pleistocene sand and gravel with clay lenses, with thickness ranging from a few meters in the south to about 400 m north (Figures 1b and S3). Moreover, the basalt and clay layer underlain the Quaternary aquifer acts as an aquiclude south of the study area, where the aquifer is thin (Figure S4). In contrast, in other areas, the Quaternary is uncomfortably underlain by the Tertiary aquifer, which is hydraulically connected particularly with the pumping increase from the Quaternary aquifer [54,55]. The consequences of the high extraction due to the irrigation of the newly reclaimed areas at the southeast corner of the study area create a cone of depression. At the same time, the increase in wastewater and surface water infiltration to the groundwater south of Shibean Elqanater City has increased the water table (Figure 1c).

The groundwater depth was measured in January 2022; it ranges from 2 m to 47 m, with the shallowest levels found near Khanka city and the deepest levels located in newly reclaimed areas southeast of the study area, at well SH35 (Figure 1a). The elevation of the water table fluctuates between 14 and −1 masl, with the highest values observed in the south and southwestern part of the study area, in the Khanka city and its vicinity. The groundwater flow direction exhibits a southwest-to-northeast pattern in the central, southern, and northern regions and a northwest-to-southeast direction in the southeastern part of the study area (Figure 1c). The groundwater recharge primarily occurs through two main sources: Nile River and irrigation canal seepage and infiltration of excess irrigation water, industrial usage, and surface water bodies (e.g., cesspools and drains) [51,56,57]. On the other hand, groundwater discharge is mainly attributed to pumping withdrawals for various purposes, such as agricultural irrigation, drinking water supply, and industrial usage.

2.2. Sample Collection

A total of 71 samples (16 surface water and 55 shallow groundwater) were collected between December 2022 and January 2023. The surface water samples were collocated as an endmember to represent the potential pollution sources for the shallow groundwater, not for water quality purposes. There are 4 samples from two different wastewater drains (Bilbies and Kalyobiya drains), 2 from Brackish lakes, 2 from agricultural drains, and 8 from surface freshwater. The majority of wells were established for private domestic purposes, with depths ranging from 9 to 43 m below the ground surface, and the average depth is 29.7 m. Each well was pumped 5 to 10 min before sampling to eliminate any stagnant water in the pipes. Of the 55 groundwater samples, 3 were from relatively deep agricultural wells (well depths of more than 50 m), and 52 were from shallow domestic wells. All samples were passed through 0.45 µm cellulose membranes and then collected into pre-washed high-density polyethylene (HDPE) bottles without headspace to avoid evaporation for the analysis of dissolved ions, heavy metals, $\delta^2H/\delta^{18}O$-H_2O, and $\delta^{15}N/\delta^{18}O$-$NO_3$. The samples were acidified for major cation and heavy metal analysis by adding a few drops of ultrapure nitric acid to lower the pH below 2 and stored in 60 mL HDPE bottles. Another 125 mL was stored in HDPE bottles for anion, $\delta^{15}N$-NO_3, and $\delta^{18}O$-NO_3 analyses. In addition, two 15 mL bottles were prepared for other anions and δ^2H-H_2O and $\delta^{18}O$-H_2O, respectively. The collected samples were carefully stored in a cold and dark environment until they can be transported back to the laboratory for analysis.

2.3. Analytical Methods

In situ measurements of water temperature (T), electrical conductivity (EC), and pH were conducted using portable pH (JENCO-6010N, USA) and EC (JENCO-EC3175, USA) meters. In addition, the HCO_3^- concentration was determined by titration within 24 h after sampling using HCl and Methyl Orange as the indicator [58]. The concentrations of Cl^-, SO_4^{2-}, F^-, SiO_2, NO_3^-, and NO_2^- were analyzed through ion chromatography (IC, DIONEX, ICS-1500, USA), with analytical precisions of ±5%. The concentration of cations

(K^+, Na^+, Mg^{2+}, and Ca^{2+}) and trace elements (As^{3+}, B^{3+}, Li^+, Sr^{3+}, Al^{3+}, Mn^{2+}, Cr^{3+}, Fe^{2+}, Co^{2+}, Cu^{2+}, Zn^{2+}, Ba^{2+}, and Ni^{2+}) were measured by an inductively coupled plasma optical emission spectrometer (ICP-OES, IRIS Intrepid II XSP, USA) with analytical precisions of ±5%. All the analyses were conducted at the Key Laboratory of Cenozoic Geology and Environment, Institute of Geology and Geophysics, Chinese Academy of Sciences, Beijing. δ^2H-H_2O and δ^{18}O-H_2O were analyzed using an IRMS at the Institute of Resources and Environment, Henan Polytechnic University, and the isotope data were reported in per mil (‰) relative to the ratios of the Vienna Standard Mean Ocean Water (VSMOW). The analytical precisions were ±0.5‰ for δ^2H and ±0.1‰ for δ^{18}O. The δ^{15}N-NO_3 and δ^{18}O-NO_3 analyses were conducted with the bacterial denitrification method [59,60]. This method examines the isotopic analysis of nitrous oxide (N_2O) reduced from NO_3^- through the activity of denitrifying bacteria that lack N_2O reductase activity, which is analyzed using an IRMS at the Environmental Stable Isotope Lab of the Chinese Academy of Agricultural Sciences. The isotope data were reported in per mil (‰) relative to atmospheric N_2 (AIR) and VSMOW. The analytical uncertainties were 0.3‰ for the δ^{15}N-NO_3^- and 0.1‰ for the δ^{18}O-NO_3^-.

3. Results and Discussion

3.1. Spatial Distribution of NO_3^- in the Shallow Groundwaters

Significant variability in NO_3^- concentrations across the studied area was observed (Figure 2a). The NO_3^- concentrations mainly ranged from 0.42 mg/L to approximately 350 mg/L, except in well SH26 (9 m depth, with a value of 651.8 mg/L). The presence of basalt at the bottom of this well acts as a NO_3^- trapping mechanism, forming a concentrated NO_3^- pool. Overall, 23.6% of the groundwater samples exceeded the permissible limit of 50 mg/L established by WHO [23]. The high NO_3^- levels were governed by unconfined conditions and the thickness of the aquifer, resulting in higher concentrations in the Abu Zaabal area (i.e., vicinity of Khanka city) at the central of the study area, extending toward the northwest and east regions following the groundwater flow path (Figure 2a). The study area was characterized into three regions based on the NO_3^- concentrations: the west, middle, and east regions. The west region exhibited low NO_3^- concentrations, which can be attributed to the dilution process from recharging by the Nile River (Damietta branch) or the presence of high thickness of the upper Holocene unit that regulates the infiltration of NO_3^- into the shallow groundwater. The middle region was generally characterized by unconfined conditions (Figure 1c), along with a small thickness of the aquifer, making it highly vulnerable to the infiltration of surface pollutants. Moreover, due to the point pollution sources (e.g., cesspools and drains), NO_3^- exhibited a wide concentration range [57,61]. Finally, the east region showed little impact from surface contaminants due to the increasing thickness of the upper Holocene layer.

3.2. Spatial Distribution of Hydrogeochemical Parameters

The hydrogeochemical parameters in the shallow groundwater aquifer exhibited a distinct spatial distribution pattern (Figures 2 and S5). The pH values ranged from 6.2 to 7.85, with a mean value of 7.08, indicating the groundwater's slightly acidic to neutral nature. The EC varied from 700 µS/cm to 3650 µS/cm, with an average of 1476 µS/cm (Table 1). The total dissolved solids (TDS), a critical indicator of dissolved chemical concentrations, exhibited a range of 455 mg/L and 2373 mg/L, with a mean value of 960 mg/L. The waters displayed elevated salinity levels, primarily attributed to the seepage of surface pollutants, particularly in the middle region. Furthermore, the increased extraction from well SH35 in the southeast part contributed to more significant mixing with the deep saline aquifer (Miocene aquifer) (Figure 2b). These observations aligned with previous studies by [55,57,62]. The SO_4^{2-} and Cl^- concentrations ranged from 2.5 mg/L to 827.2 mg/L (mean: 200.7 mg/L) and from 33.3 mg/L to 604 mg/L (mean: 170.3 mg/L), respectively. Compared with the previously reported values [61], the current study showed higher

SO_4^{2-} and Cl^- concentrations, which can be attributed to the enhanced seepage of surface pollutants, particularly notable in the middle region (Figure 2c,d).

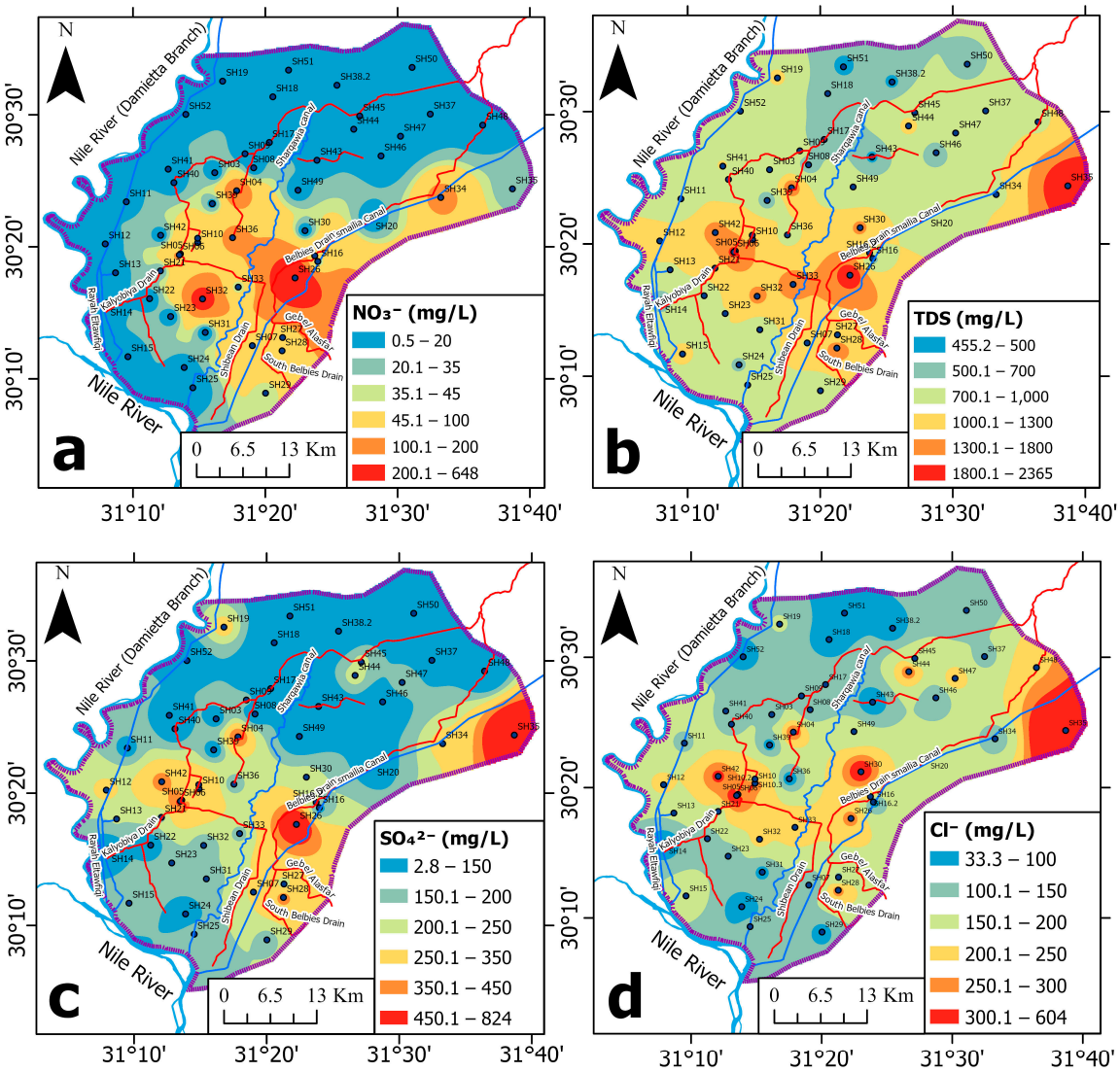

Figure 2. Spatial distribution maps of hydrogeochemical parameters of the groundwater in the study area: (**a**) TDS; (**b**) NO_3^-; (**c**) SO_4^{2-}; and (**d**) Cl^-.

The high SO_4^{2-} and Cl^- concentrations in the middle region of the study area were consistent with the high NO_3^- concentrations ($R^2 = 0.2$; $p = 0.3$ and $R^2 = 0.33$; $p < 0.01$, respectively). As SO_4^{2-} and Cl^- are typically enriched in wastewater, the correlations strengthened the scenario of increased recharge from the surface contaminant source. However, the insignificant Cl^- and NO_3^- correlation can be attributed to biochemical mediated NO_3^- concentration attenuation. In contrast, well SH35 in the southeast part records high SO_4^{2-} and Cl^- values, which can be mainly due to the mixing with the saline water from the underlain Miocene aquifer. In the west and east regions, the levels of these anions were not high, likely due to the thick upper Holocene layer in these regions and the dilution process in the west (Figure 2c,d). The HCO_3^- concentration showed high values in the west and southwest areas and decreased from the Damietta branch toward the east, with values ranging from 165.2 mg/L to 753.4 mg/L (mean: 390.9 mg/L).

Table 1. Descriptive statistics of analyzed parameters of shallow groundwater and endmember samples in the study area.

Parameter	Fresh Surface Water (n = 7)				Agricultural Drain (n = 2)				Polluted Lake (n = 2)			
	Mean	SD	Min	Max	Mean	SD	Min	Max	Mean	SD	Min	Max
Total depth (m)	–	–	–	–	–	–	–	–	–	–	–	–
pH	7.39	0.36	6.70	7.73	7.68	0.67	7.20	8.15	8.41	0.30	8.20	8.62
Temp (°C)	18.31	0.80	17.00	19.20	18.60	2.26	17.00	20.20	21.00	0.00	21.00	21.00
EC (µS/cm)	498	24	475	540	1980	665	1510	2450	17,555	1648	16,390	18,720
TDS (mg/L)	324	15	309	351	1287	432	982	1593	11,411	1071	10,654	12,168
SiO_2 (mg/L)	1.03	0.59	0.45	2.07	17.49	5.85	13.36	21.63	13.54	18.92	0.17	26.92
K^+ (mg/L)	6.10	0.42	5.66	6.60	24.58	2.84	22.57	26.60	74.11	5.17	70.45	77.76
Na^+ (mg/L)	11.74	12.45	6.46	39.97	112.21	90.13	48.48	175.94	1650	141.42	1550	1750
Ca^{2+} (mg/L)	41.09	2.01	36.77	43.05	119.63	68.46	71.22	168.03	617	316	393	840
Mg^{2+} (mg/L)	16.12	1.39	13.31	17.58	59.05	34.92	34.36	83.74	269.7	4.52	266.5	272.9
HCO_3^- (mg/L)	186.74	11.98	173.17	203.33	254.66	108.36	178.04	331.28	550.07	352.30	300.95	799.18
F^- (mg/L)	0.49	0.08	0.39	0.65	0.24	0.06	0.19	0.28	–	–	–	–
Cl^- (mg/L)	31.02	2.60	27.33	35.24	263.39	143.39	161.99	364.78	4272.9	1074.7	3513	5032.8
NO_2^- (mg/L)	–	–	–	–	–	–	–	–	–	–	–	–
NO_3^- (mg/L)	1.86	1.33	0.80	4.59	35.58	13.80	25.82	45.33	0.68	0.03	0.66	0.70
SO_4^{2-} (mg/L)	34.3	1.4	32.4	36.3	308.5	92.4	243.2	373.8	3700	132.9	3606	3794
Mn (mg/L)	0.004	0.005	0.001	0.014	0.198	0.198	0.058	0.338	0.072	0.099	0.001	0.142
Fe (mg/L)	0.045	0.005	0.037	0.053	0.137	0.093	0.071	0.203	0.171	0.004	0.168	0.174
As (mg/L)	0.0007	0.0005	0.0002	0.002	0.002	0.001	0.001	0.003	0.021	0.001	0.021	0.022
B (mg/L)	0.056	0.039	0.026	0.134	0.072	0.006	0.068	0.076	2.438	0.477	2.100	2.775
Li (mg/L)	0.001	0.0002	0.0005	0.001	0.002	0.0004	0.001	0.002	0.033	0.009	0.027	0.039
Sr (mg/L)	0.324	0.023	0.298	0.362	0.859	0.342	0.617	1.100	7.845	0.148	7.740	7.950
Al (mg/L)	0.117	0.098	0.010	0.266	0.056	0.057	0.016	0.097	0.016	0.001	0.016	0.017
Cr (mg/L)	0.011	0.001	0.009	0.013	0.011	0.002	0.010	0.012	0.033	0.023	0.017	0.050
Co (mg/L)	0.000	0.000	0.000	0.000	0.001	0.000	0.001	0.001	0.002	0.000	0.001	0.002
Cu (mg/L)	0.002	0.000	0.001	0.002	0.003	0.001	0.003	0.003	0.010	0.002	0.008	0.011
Zn (mg/L)	0.006	0.002	0.003	0.008	0.008	0.001	0.008	0.009	0.011	0.000	0.011	0.011
Ba (mg/L)	0.018	0.001	0.017	0.019	0.032	0.013	0.023	0.041	0.019	0.002	0.017	0.020
Ni (mg/L)	0.006	0.000	0.005	0.007	0.009	0.002	0.008	0.011	0.027	0.002	0.025	0.029
$\delta^{18}O$-H_2O (‰)	2.00	0.13	1.74	2.13	1.29	0.65	0.83	1.75	6.31	0.59	5.89	6.73
$\delta^{2}H$-H_2O (‰)	18.49	1.19	15.94	19.20	14.02	4.72	10.69	17.36	31.16	4.36	28.08	34.25
$\delta^{15}N$-NO_3 (‰)	5.03	8.47	−12.76	11.52	11.43	4.60	8.18	14.68	6.45	2.51	4.68	8.23
$\delta^{18}O$-NO_3 (‰)	9.02	6.65	−4.69	14.24	5.51	1.67	4.33	6.70	3.28	1.52	2.20	4.35

Table 1. *Cont.*

Parameter	Wastewater Drain (n = 4)				Groundwater (n = 55)			
	Mean	SD	Min	Max	Mean	SD	Min	Max
Total depth (m)	–	–	–	–	32.11	20.74	9.00	156.00
pH	7.24	0.48	6.56	7.70	7.08	0.36	6.20	7.75
Temp (°C)	19.38	0.85	18.50	20.50	20.29	6.63	18.50	25.30
EC (μS/cm)	1410	276	1080	1680	1476	688	700	3650
TDS (mg/L)	917	179	702	1092	960	447	455	2373
SiO_2 (mg/L)	8.99	3.65	4.16	13.02	63.53	65.57	18.70	237.32
K^+ (mg/L)	17.97	6.79	7.79	21.50	11.64	6.50	4.64	31.61
Na^+ (mg/L)	132.45	88.85	7.87	200.78	147.27	108.88	7.47	579.77
Ca^{2+} (mg/L)	62.39	11.73	46.16	71.24	102.65	49.69	19.07	366.72
Mg^{2+} (mg/L)	21.67	3.10	17.02	23.47	35.50	16.05	9.63	85.81
HCO_3^- (mg/L)	306.25	66.54	246.29	367.02	390.90	120.78	165.16	753.35
F^- (mg/L)	0.28	0.01	0.27	0.29	0.25	0.19	0.14	1.38
Cl^- (mg/L)	208.16	88.72	129.54	312.22	170.34	110.86	33.31	603.98
NO_2^- (mg/L)	107.24	63.74	50.13	176.01	–	–	–	–
NO_3^- (mg/L)	18.24	34.58	0.67	70.11	49.90	109.22	0.42	651.79
SO_4^{2-} (mg/L)	114.88	57.77	58.31	165.67	200.66	175.32	2.47	827.15
Mn (mg/L)	0.227	0.150	0.102	0.429	0.831	0.720	0.0019	3.380
Fe (mg/L)	0.088	0.020	0.069	0.108	0.089	0.060	0.040	0.430
As (mg/L)	0.001	0.001	0.001	0.002	0.002	0.001	0.000	0.006
B (mg/L)	0.137	0.038	0.090	0.177	0.094	0.112	0.016	0.577
Li (mg/L)	0.005	0.002	0.004	0.007	0.003	0.004	0.000	0.023
Sr (mg/L)	0.928	0.535	0.425	1.410	0.986	0.947	0.128	6.590
Al (mg/L)	0.030	0.005	0.024	0.036	0.012	0.006	0.007	0.046
Cr (mg/L)	0.013	0.001	0.011	0.013	0.011	0.003	0.007	0.023
Co (mg/L)	0.001	0.000	0.001	0.001	0.001	0.000	0.000	0.003
Cu (mg/L)	0.002	0.000	0.002	0.003	0.003	0.004	0.001	0.025
Zn (mg/L)	0.020	0.014	0.010	0.041	0.022	0.056	0.003	0.404
Ba (mg/L)	0.023	0.005	0.019	0.030	0.122	0.087	0.011	0.341
Ni (mg/L)	0.011	0.001	0.009	0.012	0.009	0.003	0.005	0.023
$\delta^{18}O$-H_2O (‰)	2.08	0.15	1.93	2.29	1.23	1.46	−1.86	3.32
$\delta^{2}H$-H_2O (‰)	19.10	0.87	18.19	20.20	13.99	8.83	−4.46	26.61
$\delta^{15}N$-NO_3 (‰)	8.13	6.10	−0.16	13.86	8.92	16.87	−23.40	75.42
$\delta^{18}O$-NO_3 (‰)	−1.69	13.54	−13.25	13.20	10.53	12.85	−14.32	39.79

–: not detected.

3.3. Groundwater Recharge

The stable isotopes of water ($\delta^2H/\delta^{18}O$-H_2O) provide valuable insights into the origin and movement of groundwater, rendering them indispensable tracers in hydrological investigations. The Global Meteoric Water Line (GMWL) is a crucial tool to interpret the isotopic tracers as it is a reference for understanding fractionation and mixing processes in natural water circulation [63,64]. The Nile River, irrigation canals, and drains were the potentially important shallow groundwater sources. However, before they seeped into the groundwater, the water can undergo isotopic fractionation associated with evapotranspiration during the infiltration from the ground surface, leading to enriched values. The Quaternary aquifer can be isotopically depleted because of the hydraulic connection with the depleted underlain Tertiary aquifer.

The stable isotope composition of water samples gathered from the study area is depicted on the conventional $\delta^{18}O$-H_2O and δ^2H-H_2O diagram (Figure 3). The groundwater values for $\delta^{18}O$-H_2O and δ^2H-H_2O exhibit considerable diversity, spanning from −1.86‰ to 3.32‰ and from −4.46‰ to 26.61‰, respectively (Table 1). The water samples deviate below the GMWL (Figure 3), suggesting that they had been influenced by evaporation, in contrast with the old Nile water sample before Aswan High Dam (AHD) compiled by [65], which was distributed close to the GMWL. Most of the samples were distributed near the Nile water, the irrigation return flow, and wastewater endmembers (Figure 3), suggesting that these sources primarily recharged the shallow groundwater.

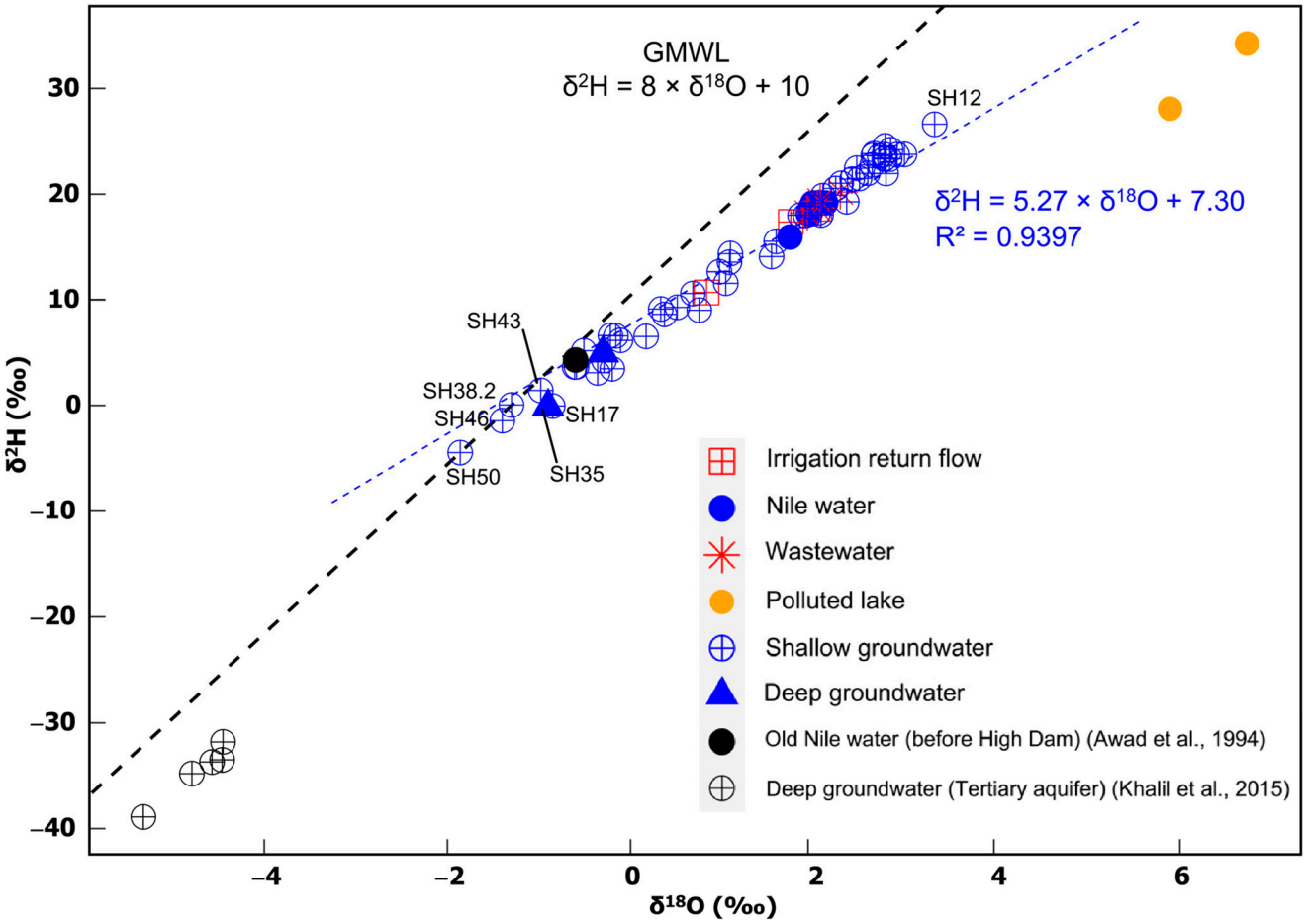

Figure 3. Scatterplot of water staple isotopes (δ^2H-H_2O and $\delta^{18}O$-H_2O) in groundwater and end-member samples in the study area [55,65].

In particular, the groundwater in the middle and western regions of the study area has undergone modern recharge, as indicated by its isotopic composition closely resembling

that of the Nile water. In the west region, the isotopic values of groundwater experienced noticeable enrichment, likely due to an increase in evaporation (Figure 4). Several factors can contribute to this phenomenon. Firstly, the availability of Nile water and the prevalent traditional irrigation method, such as flood irrigation, enhance evaporation due to prolonged time on the surface before seeping downward. Secondly, the shallow depth of the water table contributed to the enrichment of the isotopic signature. Lastly, the presence of a thick upper Holocene unit exacerbated the evaporation process. Conversely, in the middle region, where this layer was absent, and there was a shortage of Nile water coupled with increased groundwater abstraction to compensate for this shortage, the isotopic composition of the groundwater remained closer to that of the Nile water and drainage systems. In the east region, where the upper Holocene layer is thick and there is shortage of the Nile water, the abstraction of the groundwater increased, which resulted in well nos. SH43, SH17, SH35, SH50, SH46, and SH38.2 being affected by mixing with the Tertiary aquifer. These findings are consistent with previous studies conducted by [51,66]. These results show that, although the NO_3^- groundwater pollution in the west/east regions was low, it can result from irrigation water enriched with CF and SON. This low concentration was due to the dilution of excess irrigation water and the Nile water recharging in the west.

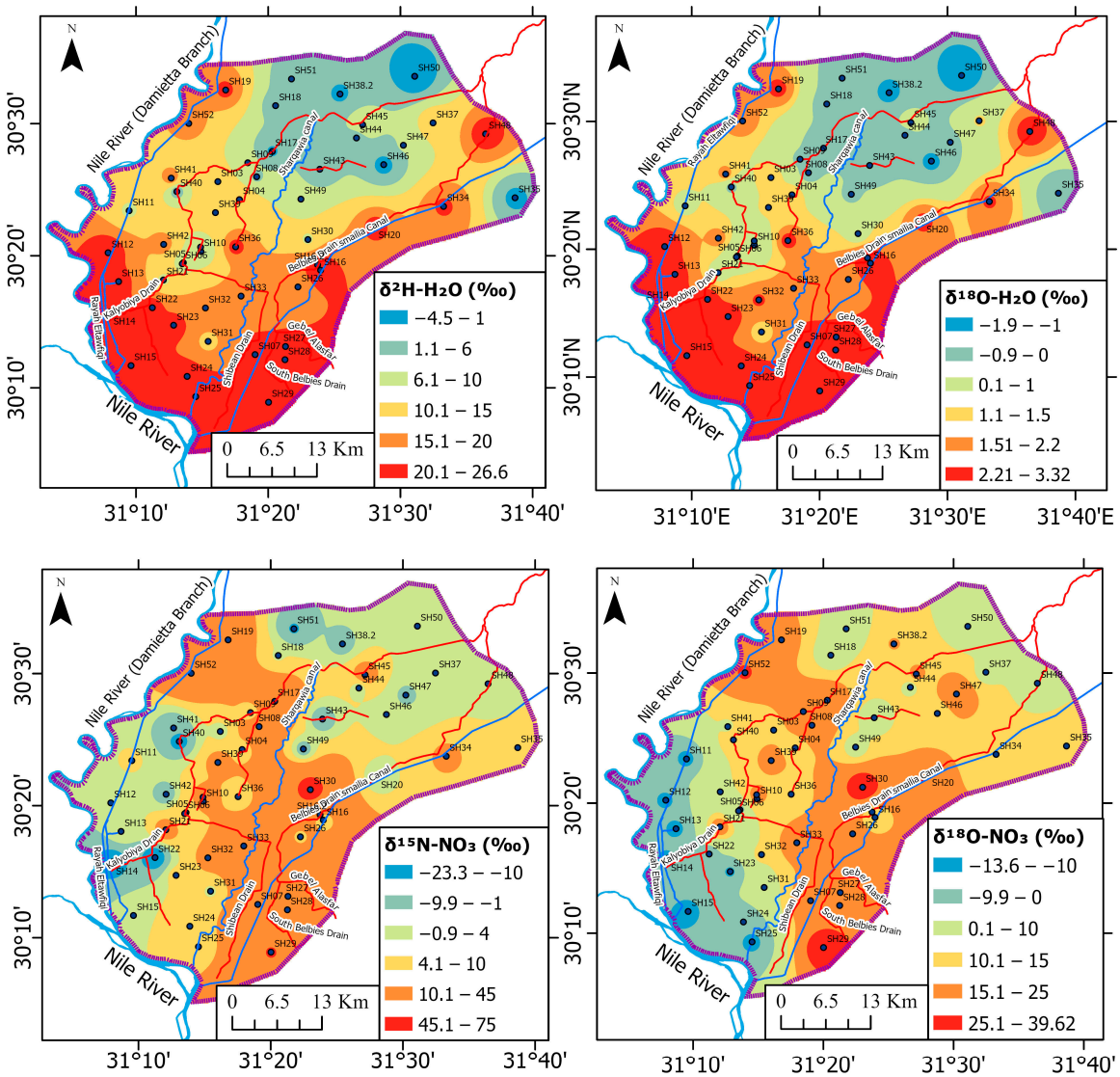

Figure 4. Spatial distribution maps of the δ^2H-H_2O, δ^{18}O-H_2O, δ^{15}N-NO_3, and δ^{18}O-NO_3 of the groundwater in the study area.

In contrast, in the east, the dilution that resulted from the mixing with the deep groundwater contributed to the low NO_3^- concentrations. However, the relatively high NO_3^- (28.8 mg/L in well SH35) southeast of the study area could have originated from the lateral groundwater flow with high NO_3^- concentration due to relatively intense abstraction (250 m3/day). In contrast, in the middle region, more wastewater is loaded into the groundwater due to unconfined conditions.

3.4. Sources and Transformations of NO_3^-

Cl^- serves as a reliable indicator of wastewater and fertilizer impacts, which can contribute to elevated Cl^- levels and is unaffected by chemical, physical, and biological processes [45,46,67]. The correlation between Cl^- and NO_3^-/Cl^- is widely utilized for source identification of NO_3^- sources in water, specifically for distinguishing agricultural or/and wastewater sources [45,47] and for distinguishing between the influences of dilution and denitrification on NO_3^- levels [68]. A high NO_3^-/Cl^- ratio coupled with low Cl^- levels indicates that agricultural sources (e.g., chemical fertilizer) and soil organic nitrogen (SON) are the main contributors of NO_3^- in the groundwater. Conversely, a low NO_3^-/Cl^- ratio and high Cl^- content suggest wastewater sources as the primary origin of NO_3^- contamination [27,69].

Most of the groundwater samples had NO_3^-/Cl^- ratios < 1 and relatively high Cl^- concentrations (Figure 5a), suggesting a probable dominance of wastewater as the NO_3^- source [68,70]. However, a few samples in the middle region (SH26 and SH36; Figure 5a) exhibited high NO_3^-/Cl^- ratios > 1, which can be linked to a combination of SON and CF with wastewater inputs [70] (Figure 5a). The significant correlation between SO_4^{2-} and NO_3^- of the groundwaters in the middle region supported the dominant role of wastewater (Figures 5b and 6b) [71–73]. A few points were scattered from the correlation, which can be ascribed to the evaporate (e.g., gypsum) dissolution in the arid region [74,75] or as a result of using CF enriched with SO_4^{2-} [13,76].

In addition, most of the groundwater samples in the study area exhibited TDS concentrations below 1000 mg/L associated with a low $(NO_3^- + Cl^-)/HCO_3^-$ ratio. The correlation is strongly positive ($R^2 = 0.71$; $p < 0.01$) in the middle region, which can be attributed to the substantial reduction condition and then denitrification, which attenuates the NO_3^- and/or produce more HCO_3^- [70,77] (Figure 5c). This speculation can then be consistent with the theoretical denitrification defined in Equation (1) [78,79]. In the west and east regions, this relationship is a weak positive correlation as a result of the impacts of SON and CF [73,80] associated with biodegradation of organic matter, which is rich in the upper Holocene layer in these regions and consequently increase HCO_3^- concentration [81].

$$NO_3^- + 1.08\ CH_3OH + 0.24\ H_2CO_3 \rightarrow 0.56\ C_5H_7O_2N + 0.47\ N_2 + HCO_3^- + 1.68\ H_2O \quad (1)$$

The dual NO_3^- isotope approach ($\delta^{15}N\text{-}NO_3$ and $\delta^{18}O\text{-}NO_3$) is widely recognized as a powerful technique for constraining NO_3^- sources and behaviors [9,38,45,50,82]. Different NO_3^- sources exhibit characteristic isotopic signatures of $\delta^{15}N\text{-}NO_3$ and $\delta^{18}O\text{-}NO_3$, which can be used to trace their origins [38,83,84]. Figure 7a shows the $\delta^{15}N\text{-}NO_3$ and $\delta^{18}O\text{-}NO_3$ values of the groundwaters, Nile water, and potential endmembers in the study area. The isotopic compositions of $\delta^{15}N\text{-}NO_3$ and $\delta^{18}O\text{-}NO_3$ in the groundwaters showed wide ranges, ranging from −23.4‰ to 75.4‰ (mean: 8.92‰) and from −14.3‰ to 39.8‰ (mean: 10.53‰), respectively (Table 1). The groundwaters in the middle region have $\delta^{15}N\text{-}NO_3$ and $\delta^{18}O\text{-}NO_3$ ranging from 4‰ to 24.4‰ and from 10‰ to 23.9‰, respectively (Figures 4 and 7). As expected, the data are distributed near the endmembers for SON and CF and wastewater, suggesting that these anthropogenic sources should be the major sources of the groundwaters (Figure 7a). Due to their analogous isotopic compositions and transport routes, we merged SON and CF as one source. The direct input of atmospheric precipitation should be minor because the study area experiences minimal precipitation (Figure 7a).

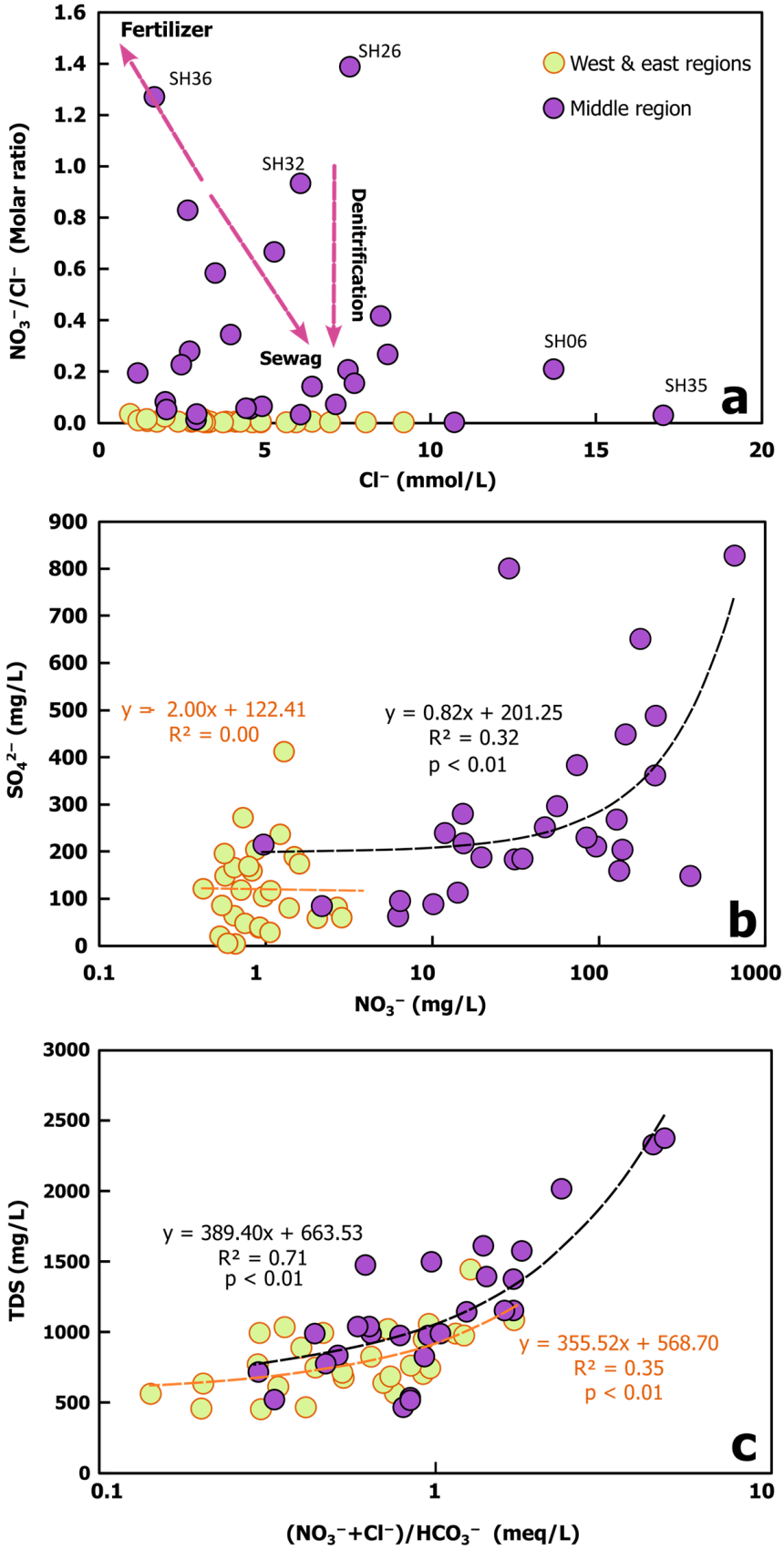

Figure 5. Plot of (**a**) NO_3^- + Cl^- versus Cl^-; (**b**) NO_3^- versus SO_4^{2-}; and (**c**) TDS versus (NO_3^- + Cl^-)/HCO_3^- of the groundwater samples in the study area.

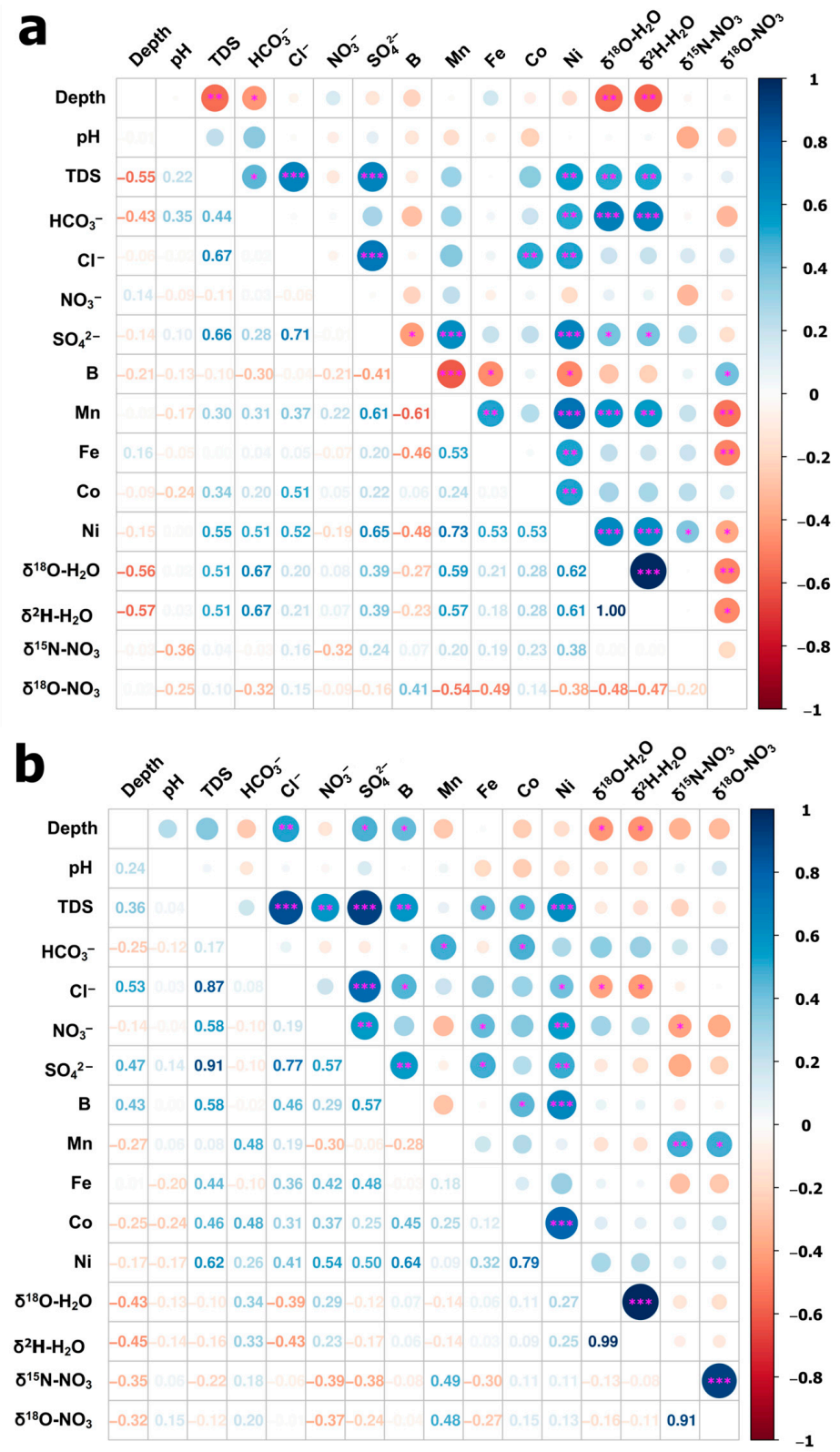

Figure 6. Plot of the Pearson correlation matrix of hydrogeochemical and isotope data of the shallow groundwater in the (**a**) west/east regions and (**b**) middle region. * $p < 0.05$; ** $p < 0.01$; *** $p < 0.001$.

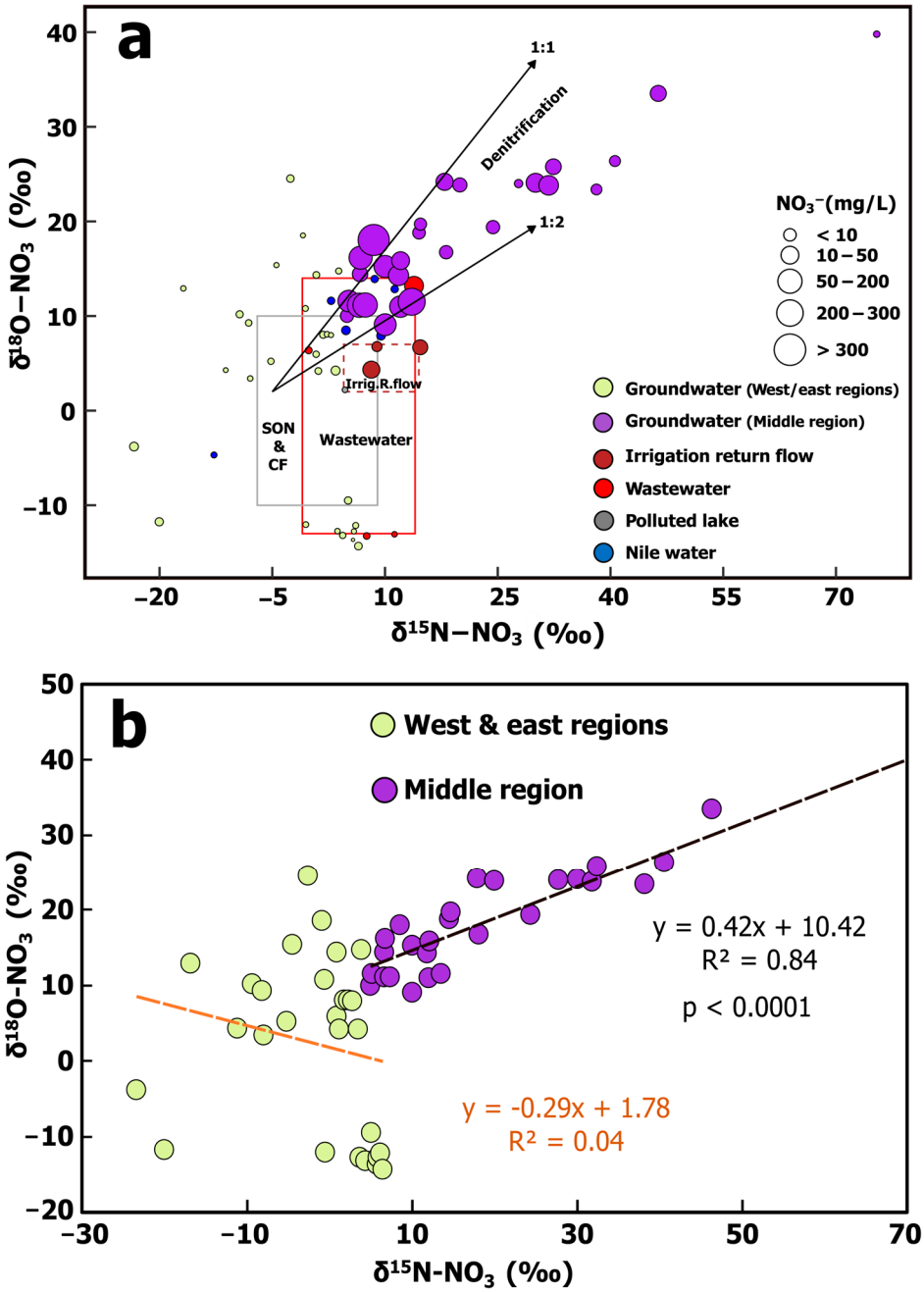

Figure 7. (**a**) Relationship between δ^{15}N-NO_3 and δ^{18}O-NO_3 values of the groundwater and endmember samples, with the ranges of potential nitrate sources. (**b**) δ^{15}N-NO_3 versus δ^{18}O-NO_3 of the groundwater samples in the study area.

Notably, a number of the isotopic values, especially those in the middle region, are higher than all the endmembers, and there is a significant positive correlation between the dual isotopes with a slope of 0.48 ($R^2 = 0.39$, $p < 0.0001$) (Figures 4, 6b and 7), which is the typical isotopic signal for biological NO_3^- removal [38]. Denitrification in groundwaters is well documented, leading to an exponential co-increase in δ^{15}N-NO_3 and δ^{18}O-NO_3, with values exceeding 100‰ recorded [38]. The significant denitrification is also supported by the simultaneous decreasing NO_3^- levels and increasing dual isotopic values (Figures 6b and 7a). The observation gives us the confidence that the prevalent denitrification process counterbalanced the excess NO_3^- loading to the groundwater to some extent (Figure 7a). The presence of clay lenses and clayey sediments in the aquifer can enhance the

denitrification [38,85] by providing soluble organic carbon and anaerobic conditions [77]. However, more excess NO_3^- loading into the groundwater can inhibit this process and result in high NO_3^- levels (e.g., SH26 and SH32).

By contrast, no relationships existed between the dual isotopes in the samples collected in the west/east regions (Figures 6a and 7b), indicating minor denitrification. The groundwater samples in the west and east regions exhibited relatively depleted and constrained δ^{15}N-NO_3 values (Figures 4 and 7a). Their δ^{15}N-NO_3 and δ^{18}O-NO_3 compositions ranged from −23.3‰ to 4‰ and from −13.6‰ to 10‰, respectively. Most of these samples had δ^{15}N-NO_3 values lower than most ^{15}N-depleted SON and CF endmember, which can be ascribed to nitrification processes. Nitrification has a substantial fractionation effect, with ^{14}N being preferentially nitrified in NH_4^+ plentiful environments. The anthropogenic activities should discharge a large amount of NH_4^+ containing wastewater and irrigation discharge to the groundwaters, resulting in NH_4^+ plentiful conditions. Yet, the overall anaerobic environments in the groundwaters would inhibit nitrification. The speculation is supported by the low NO_3^- concentrations (Figures 4 and 7a). Collectively, the low isotopic values and concentrations of NO_3^- in the west/east regions should be attributed to the nitrification process, which also can be enhanced in the west due to the long residence time of water on the surface before it seeps into the groundwater [86]. Notably, although sample SH35 is collected from a deep well (depth = 156 m), it showed a NO_3^- value of 28.8 mg/L; this observation can result from NO_3^- recharging to the deep zone through the lateral groundwater flow.

Overall, according to the water chemistry and isotopic tracers, we found that wastewater and SON and CF were the major sources of shallow groundwaters. Denitrification is the primary process that occurs in the middle region accompanied by excess NO_3^- loadings, whereas the west/east regions can be affected by zonal nitrification.

3.5. Identification of NO_3^- Transformation Process Coupled with Mn Oxides Reduction

The presence of trace elements in groundwater provides valuable insights into NO_3^- dynamics [12,87]. Among these trace elements, Mn^{2+}, Fe^{2+}, and Cu^{2+} play crucial roles in denitrification by enhancing the rate of this process [44]. Notably, the relationship between oxidation and reduction of Mn and Fe in natural waters extends beyond the typical redox conditions necessary for their mobilization [88]. Mn and Fe in minerals serve as electron acceptors for denitrifying bacteria [77], thereby facilitating denitrification and ultimately enhancing denitrification rates [43,44,89].

The concentrations of Mn^{2+} in the groundwaters ranged from 0.002 mg/L to 3.38 mg/L, with a mean value of 0.83 mg/L. Furthermore, it is noteworthy that 65.5% of the groundwater samples examined exceeded the permissible limit of 0.4 mg/L set by the WHO (Figure S6). There were significant correlations between the Mn^{2+} concentrations and the δ^{15}N-NO_3 and δ^{18}O-NO_3 values in the middle region ($p < 0.01$; Figures 6b and 8a,b), implying the role of Mn in regulating the prevalent denitrification. The speculation was also supported by the negative correlation between Mn^{2+} and NO_3^- concentrations (Figures 6b and 8c). In addition, in the west/east region, the above correlations were absent (Figures 6a and 8a,c), further giving us the confidence that the biogeochemistry of Mn and denitrification were tightly coupled. This observed relationship was in line with the results of an experimental study that showed that MnO_2 addition enhanced the denitrifying bacteria's metabolism and removed about 99% of the NO_3^- and released Mn^{2+} in weak acidic and neutral conditions [43].

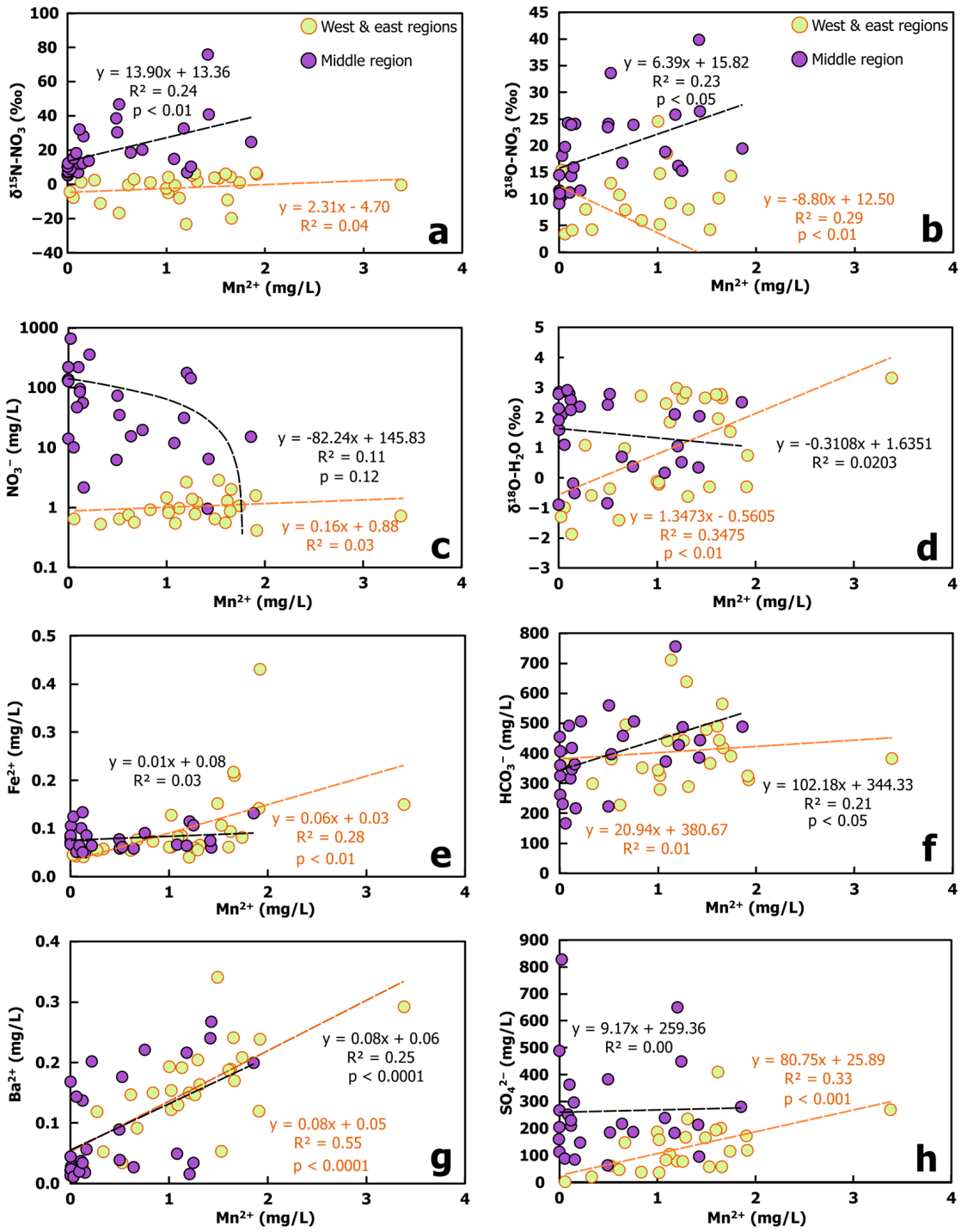

Figure 8. Scatterplot of (**a**) Mn^{2+} versus $\delta^{15}N\text{-}NO_3$; (**b**) Mn^{2+} versus $\delta^{18}O\text{-}NO_3$; (**c**) Mn^{2+} versus NO_3^-; (**d**) Mn^{2+} versus $\delta^{18}O\text{-}H_2O$; (**e**) Mn^{2+} versus Fe^{2+}; (**f**) Mn^{2+} versus HCO_3^-; (**g**) Mn^{2+} versus Ba^{2+}; and (**h**) Mn^{2+} versus SO_4^{2-} of the groundwater in this study.

The potential source of Mn in the study area is the upper Holocene layer [90], which is also enriched in organic matter and Mn minerals, leading to reduced environments [91]. Mn is commonly present in insoluble Mn(IV) and Mn(III), and their reduction will generate soluble Mn^{2+} [88,90]. In addition, Mn can result from CF utilized in the fruit farms in the western region [92]. We observed co-increasing of Mn^{2+} with HCO_3^-, Fe^{2+}, and Ba^{2+} (Figures 6 and 8e–g). As HCO_3^-, Fe^{2+}, and Ba^{2+} concentrations are closely related to chemical weathering, high Mn^{2+} in the groundwaters should be associated with chemical

weathering processes. The mafic rocks are enriched with Mn [88] and the origin of the Nile silts and the Quaternary deposits as a result of weathering of these rocks [93], which lead to sediment enriched with Mn oxides. In contrast, there was no significant relationship between Mn^{2+} and SO_4^{2-} in the middle region (Figures 6b and 8h), indicating that the anthropogenic contribution of Mn^{2+} was less significant. However, Mn^{2+} and SO_4^{2-} showed a significant positive correlation in the west/east regions (Figures 6a and 8h), indicating the direct input of Mn^{2+} from anthropogenic sources [81,91]. That is, Mn was largely in an oxidized form in this layer before entering the water body, and it cannot participate in the reduction of NO_3^-. As the predominant factors influencing the concentrations of Mn^{2+} in the shallow groundwaters in the west/east and middle regions of the study area are quite different, the increase in Mn^{2+} concentrations and the associated redox process in the middle region enhanced denitrification, while in the west/east regions, denitrification and Mn^{2+} concentrations were decoupled.

However, reducing the Fe/Mn oxides coupled with nitrification–denitrification under anaerobic conditions and replacing the need for O_2 can be prevalent in these areas, where NH_4^+ oxidized and turned to NO_3^- or N_2 (i.e., anammox) based on Equation (2) [78].

$$NH_4^+ + 1.31\ NO_2^- + 0.066\ HCO_3^- + 0.13\ H^+ \rightarrow 1.02\ N_2 + 0.26\ NO_3^- + 0.066\ CH_2O_{0.5}N_{0.15} + 2.03\ H_2O \quad (2)$$

These findings highlight the importance of considering the biogeochemistry of trace elements, particularly Mn^{2+}, in assessing and managing NO_3^- contamination in shallow groundwater. However, it is important to note that while denitrification mitigates NO_3^- excess, it cannot fully offset the increasing NO_3^- loading into the groundwater. Due to this process, there is a higher release of Mn^{2+}, which, when combined with an excess of NO_3^-, poses a potential health risk to the residents.

4. Conclusions

In the present investigation, the hydrogeochemical parameters and multi-isotope tracers were used to identify the sources and transformation of NO_3^- in the shallow groundwater in the southeast of the Nile Delta region for the first time. Our findings reveal that the NO_3^- values ranged from 0.42 mg/L to 650 mg/L and the groundwater in the middle region was highly impacted by NO_3^- pollution. The NO_3^- pollution in the west/east regions was relatively weak due to a thick upper Holocene layer or as a result of the dilution process by the Nile River recharge in the west or the mixing with deep groundwater in the east. According to the WHO guidelines for drinking water, the criterion for NO_3^- and Mn^{2+} is exceeded in 23.6% and 65.5% of shallow groundwater samples, respectively. The values of δ18O-NO_3 and δ15N-NO_3 between −14.32‰ and −39.79‰ and between −23.4‰ and –75.42‰, respectively, implied that wastewater and SON and CF were the main NO_3^- sources. NO_3^- in the west/east regions can be derived from SON and CF associated with zonal nitrification. While in the middle region, NO_3^- was more derived from the wastewater, and the denitrification was prevalent. Remarkably, the denitrification might be closely coupled with the biogeochemical cycling of Mn. Finally, the data obtained from this study bear significant implications across several dimensions. Firstly, it establishes the first reference for NO_3^- isotope investigations of the groundwater in Egypt. Secondly, it is poised to furnish valuable insights to coupling Mn^{+2} and NO_3^- biogeochemical dynamics in the arid region, delineating pivotal denitrification and Mn reduction relationships.

Supplementary Materials: The following supporting information can be downloaded at: https://www.mdpi.com/article/10.3390/w16010022/s1. Figure S1: Geology of the southeastern region of the Nile Delta; Figure S2: Land use/Land cover (LU/LC) 10 m resolution (year 2022) of the study area; Figure S3: Hydrogeological map of the study area; Figure S4: Hydrogeological cross-section A-A′; Figure S5: Spatial distribution maps of the groundwater in the study area: (a) EC; (b) pH; (c) Na^+; (d) HCO_3^-; Figure S6: Spatial distribution maps of the groundwater in the study area: (a) Ca^{2+}; (b) Mg^{2+}; (c) Mn^{2+}; (d) Fe^{2+}; Figure S7: Scatterplot of Mn^{2+} versus SO_4^{2-}/Cl^- of the groundwater in

the study area; Figure S8: Scatterplot of (a) ln [NO_3^-] versus δ^{18}O-NO_3, (b) ln [NO_3^-] versus δ^{15}N-NO_3 of the groundwater in the middle region of the study area; Figure S9: Scatterplot of (a) ln [NO_3^-] versus δ^{18}O-NO_3, (b) ln [NO_3^-] versus δ^{15}N-NO_3 of the groundwater in the west/east regions of the study area; Table S1: Quality parameters of the groundwater samples in the study area; Table S2: Limit of Detection of the Inductively Coupled Plasma Optical Emission Spectrometer (ICP-OES, IRIS Intrepid II XSP, USA) and ion chromatography (IC, Dionex 120, USA). References [23,53,54,94–96] are cited in the Supplementary Materials.

Author Contributions: Conceptualization, A.M.K., Z.X. and W.L.; methodology, A.M.K., Z.X. and W.L.; formal analysis, A.M.K., H.J., W.L. and J.Z.; investigation, A.M.K. and A.M.N.; writing—original draft preparation, A.M.K.; writing—review and editing, A.M.K., Z.X., H.J., W.L., J.Z. and A.M.N.; supervision, Z.X.; funding acquisition, Z.X. All authors have read and agreed to the published version of the manuscript.

Funding: This research was financially supported by the National Key Research and Development Program of China (grant no. 2020YFA0607700), the National Natural Science Foundation of China (grant nos. 41730857 and 42273050), and the Key Research Program of the Institute of Geology & Geophysics, CAS (grant no. IGGCAS-202204). Wenjing Liu acknowledges support from the Youth Innovation Promotion Association CAS (2019067).

Data Availability Statement: Data are available on request.

Acknowledgments: Alaa M. Kasem would like to thank the CAS-TWAS President's Fellowship Programme.

Conflicts of Interest: The authors declare that they have no known competing financial interest or personal relationship that could have appeared to influence the work reported in this paper.

References

1. Li, P.; Karunanidhi, D.; Subramani, T.; Srinivasamoorthy, K. Sources and Consequences of Groundwater Contamination. *Arch. Environ. Contam. Toxicol.* **2021**, *80*, 1–10. [CrossRef] [PubMed]
2. Han, G.; Tang, Y.; Liu, M.; Van Zwieten, L.; Yang, X.; Yu, C.; Wang, H.; Song, Z. Carbon-Nitrogen Isotope Coupling of Soil Organic Matter in a Karst Region under Land Use Change, Southwest China. *Agric. Ecosyst. Environ.* **2020**, *301*, 107027. [CrossRef]
3. Breida, M.; Alami Younssi, S.; Ouammou, M.; Bouhria, M.; Hafsi, M. Pollution of Water Sources from Agricultural and Industrial Effluents: Special Attention to NO_3^-, Cr(VI), and Cu(II). In *Water Chemistry*; IntechOpen: Rijeka, Croatia, 2020.
4. Zendehbad, M.; Cepuder, P.; Loiskandl, W.; Stumpp, C. Source Identification of Nitrate Contamination in the Urban Aquifer of Mashhad, Iran. *J. Hydrol. Reg. Stud.* **2019**, *25*, 100618. [CrossRef]
5. Zhang, Q.; Miao, L.; Wang, H.; Hou, J.; Li, Y. How Rapid Urbanization Drives Deteriorating Groundwater Quality in a Provincial Capital of China. *Pol. J. Environ. Stud.* **2019**, *29*, 441–450. [CrossRef] [PubMed]
6. Han, G.; Liu, C.Q. Water Geochemistry Controlled by Carbonate Dissolution: A Study of the River Waters Draining Karst-Dominated Terrain, Guizhou Province, China. *Chem. Geol.* **2004**, *204*, 1–21. [CrossRef]
7. El Shinawi, A.; Zeleňáková, M.; Nosair, A.M.; Abd-Elaty, I. Geo-Spatial Mapping and Simulation of the Sea Level Rise Influence on Groundwater Head and Upward Land Subsidence at the Rosetta Coastal Zone, Nile Delta, Egypt. *J. King Saud. Univ. Sci.* **2022**, *34*, 102145. [CrossRef]
8. Elewa, H.H.; Shohaib, R.E.; Qaddah, A.A.; Nousir, A.M. Determining Groundwater Protection Zones for the Quaternary Aquifer of Northeastern Nile Delta Using GIS-Based Vulnerability Mapping. *Environ. Earth Sci.* **2013**, *68*, 313–331. [CrossRef]
9. Gutiérrez, M.; Biagioni, R.N.; Alarcón-Herrera, M.T.; Rivas-Lucero, B.A. An Overview of Nitrate Sources and Operating Processes in Arid and Semiarid Aquifer Systems. *Sci. Total Environ.* **2018**, *624*, 1513–1522. [CrossRef]
10. Huang, T.; Pang, Z.; Yuan, L. Nitrate in Groundwater and the Unsaturated Zone in (Semi)Arid Northern China: Baseline and Factors Controlling Its Transport and Fate. *Environ. Earth Sci.* **2013**, *70*, 145–156. [CrossRef]
11. Li, P.; Tian, R.; Xue, C.; Wu, J. Progress, Opportunities, and Key Fields for Groundwater Quality Research under the Impacts of Human Activities in China with a Special Focus on Western China. *Environ. Sci. Pollut. Res.* **2017**, *24*, 13224–13234. [CrossRef]
12. Arcega-Cabrera, F.; Sickman, J.O.; Fargher, L.; Herrera-Silveira, J.; Lucero, D.; Oceguera-Vargas, I.; Lamas-Cosío, E.; Robledo-Ardila, P.A. Groundwater Quality in the Yucatan Peninsula: Insights from Stable Isotope and Metals Analysis. *Groundwater* **2021**, *59*, 878–891. [CrossRef] [PubMed]
13. Biddau, R.; Dore, E.; Da Pelo, S.; Lorrai, M.; Botti, P.; Testa, M.; Cidu, R. Geochemistry, Stable Isotopes and Statistic Tools to Estimate Threshold and Source of Nitrate in Groundwater (Sardinia, Italy). *Water Res.* **2023**, *232*, 119663. [CrossRef] [PubMed]
14. Ibrahim, K.O.; Gomo, M.; Oke, S.A. Groundwater Quality Assessment of Shallow Aquifer Hand Dug Wells in Rural Localities of Ilorin Northcentral Nigeria: Implications for Domestic and Irrigation Uses. *Groundw. Sustain. Dev.* **2019**, *9*, 100226. [CrossRef]

15. Jakeman, A.J.; Barreteau, O.; Hunt, R.J.; Rinaudo, J.-D.; Ross, A.; Arshad, M.; Hamilton, S. *Integrated Groundwater Management: An Overview of Concepts and Challenges in Integrated Groundwater Management: Concepts, Approaches and Challenges*; Jakeman, A.J., Barreteau, O., Hunt, R.J., Rinaudo, J.-D., Ross, A., Eds.; Springer International Publishing: Cham, Switzerland, 2016; pp. 3–20, ISBN 978-3-319-23576-9.
16. Puckett, L.J. *Nonpoint and Point Sources of Nitrogen in Major Watersheds of the United States*; Water-Resources Investigations Report 94-4001; US Geological Survey: Menlo Park, CA, USA, 1994; Volume 94.
17. Wakida, F.T.; Lerner, D.N. Non-Agricultural Sources of Groundwater Nitrate: A Review and Case Study. *Water Res.* **2005**, *39*, 3–16. [CrossRef] [PubMed]
18. Zhang, Q.; Sun, J.; Liu, J.; Huang, G.; Lu, C.; Zhang, Y. Driving Mechanism and Sources of Groundwater Nitrate Contamination in the Rapidly Urbanized Region of South China. *J. Contam. Hydrol.* **2015**, *182*, 221–230. [CrossRef] [PubMed]
19. Davidson, E.A.; David, M.B.; Galloway, J.N.; Goodale, C.L.; Haeuber, R.; Harrison, J.A.; Howarth, R.W.; Jaynes, D.B.; Lowrance, R.R.; Thomas, N.B.; et al. Excess Nitrogen in the U.S. Environment: Trends, Risks, and Solutions. *Issues Ecol.* **2011**, *15*, 1–16.
20. Dan-Hassan, M.A.; Olasehinde, P.I.; Amadi, A.N.; Yisa, J.; Jacob, J.O. Spatial and Temporal Distribution of Nitrate Pollution in Groundwater of Abuja, Nigeria. *Int. J. Chem.* **2012**, *4*, 104–112. [CrossRef]
21. Ward, M.H.; de Kok, T.M.; Levallois, P.; Brender, J.; Gulis, G.; Nolan, B.T.; VanDerslice, J. Workgroup Report: Drinking-Water Nitrate and Health—Recent Findings and Research Needs. *Environ. Health Perspect.* **2018**, *113*, 1607–1614. [CrossRef]
22. Jia, H.; Howard, K.; Qian, H. Use of Multiple Isotopic and Chemical Tracers to Identify Sources of Nitrate in Shallow Groundwaters along the Northern Slope of the Qinling Mountains, China. *Appl. Geochem.* **2020**, *113*, 104512. [CrossRef]
23. WHO. *Guidelines for Drinking Water Quality*; Fourth Edition Incorporating The First Addendum; World Health Organization: Geneva, Switzerland, 2017.
24. Rahman, A.; Mondal, N.C.; Tiwari, K.K. Anthropogenic Nitrate in Groundwater and Its Health Risks in the View of Background Concentration in a Semi Arid Area of Rajasthan, India. *Sci. Rep.* **2021**, *11*, 9279. [CrossRef]
25. Shakerkhatibi, M.; Mosaferi, M.; Pourakbar, M.; Ahmadnejad, M.; Safavi, N.; Banitorab, F. Comprehensive Investigation of Groundwater Quality in the North-West of Iran: Physicochemical and Heavy Metal Analysis. *Groundw. Sustain. Dev.* **2019**, *8*, 156–168. [CrossRef]
26. Šrajbek, M.; Kranjčević, L.; Kovač, I.; Biondić, R. Groundwater Nitrate Pollution Sources Assessment for Contaminated Wellfield. *Water* **2022**, *14*, 255. [CrossRef]
27. Romanelli, A.; Soto, D.X.; Matiatos, I.; Martínez, D.E.; Esquius, S. A Biological and Nitrate Isotopic Assessment Framework to Understand Eutrophication in Aquatic Ecosystems. *Sci. Total Environ.* **2020**, *715*, 136909. [CrossRef]
28. Pastén-Zapata, E.; Ledesma-Ruiz, R.; Harter, T.; Ramírez, A.I.; Mahlknecht, J. Assessment of Sources and Fate of Nitrate in Shallow Groundwater of an Agricultural Area by Using a Multi-Tracer Approach. *Sci. Total Environ.* **2014**, *470–471*, 855–864. [CrossRef] [PubMed]
29. Lee, C.M.; Choi, H.; Kim, Y.; Kim, M.S.; Kim, H.K.; Hamm, S.Y. Characterizing Land Use Effect on Shallow Groundwater Contamination by Using Self-Organizing Map and Buffer Zone. *Sci. Total Environ.* **2021**, *800*, 149632. [CrossRef]
30. Chen, R.; Hu, Q.; Shen, W.; Guo, J.; Yang, L.; Yuan, Q.; Lu, X.; Wang, L. Identification of Nitrate Sources of Groundwater and Rivers in Complex Urban Environments Based on Isotopic and Hydro-Chemical Evidence. *Sci. Total Environ.* **2023**, *871*, 162026. [CrossRef]
31. Hosono, T.; Tokunaga, T.; Kagabu, M.; Nakata, H.; Orishikida, T.; Lin, I.-T.; Shimada, J. The Use of Δ15N and Δ18O Tracers with an Understanding of Groundwater Flow Dynamics for Evaluating the Origins and Attenuation Mechanisms of Nitrate Pollution. *Water Res.* **2013**, *47*, 2661–2675. [CrossRef]
32. Jin, Z.; Qin, X.; Chen, L.; Jin, M.; Li, F. Using Dual Isotopes to Evaluate Sources and Transformations of Nitrate in the West Lake Watershed, Eastern China. *J. Contam. Hydrol.* **2015**, *177–178*, 64–75. [CrossRef]
33. Lorette, G.; Sebilo, M.; Buquet, D.; Lastennet, R.; Denis, A.; Peyraube, N.; Charriere, V.; Studer, J.-C. Tracing Sources and Fate of Nitrate in Multilayered Karstic Hydrogeological Catchments Using Natural Stable Isotopic Composition (Δ15N-NO_3^- and Δ18O-NO_3^-). Application to the Toulon Karst System (Dordogne, France). *J. Hydrol.* **2022**, *610*, 127972. [CrossRef]
34. Xing, M.; Liu, W. Using Dual Isotopes to Identify Sources and Transformations of Nitrogen in Water Catchments with Different Land Uses, Loess Plateau of China. *Environ. Sci. Pollut. Res.* **2016**, *23*, 388–401. [CrossRef]
35. Yue, F.-J.; Li, S.-L.; Liu, C.-Q.; Zhao, Z.-Q.; Ding, H. Tracing Nitrate Sources with Dual Isotopes and Long Term Monitoring of Nitrogen Species in the Yellow River, China. *Sci. Rep.* **2017**, *7*, 8537. [CrossRef] [PubMed]
36. Zhang, Q.; Wang, H.; Wang, L. Tracing Nitrate Pollution Sources and Transformations in the Over-Exploited Groundwater Region of North China Using Stable Isotopes. *J. Contam. Hydrol.* **2018**, *218*, 1–9. [CrossRef] [PubMed]
37. Zhang, Y.; Li, F.; Zhang, Q.; Li, J.; Liu, Q. Tracing Nitrate Pollution Sources and Transformation in Surface- and Ground-Waters Using Environmental Isotopes. *Sci. Total Environ.* **2014**, *490*, 213–222. [CrossRef] [PubMed]
38. Kendall, C.; Elliott, E.M.; Wankel, S.D. Tracing Anthropogenic Inputs of Nitrogen to Ecosystems. In *Stable Isotopes in Ecology and Environmental Science*, 2nd ed.; Michener, R., Lajtha, K., Eds.; Blackwell Publishing Ltd.: Oxford, UK, 2007; pp. 375–449.
39. Spalding, R.F.; Hirsh, A.J.; Exner, M.E.; Little, N.A.; Kloppenborg, K.L. Applicability of the Dual Isotopes Δ15N and Δ18O to Identify Nitrate in Groundwater beneath Irrigated Cropland. *J. Contam. Hydrol.* **2019**, *220*, 128–135. [CrossRef] [PubMed]
40. Cao, M.; Hu, A.; Gad, M.; Adyari, B.; Qin, D.; Zhang, L.; Sun, Q.; Yu, C.P. Domestic Wastewater Causes Nitrate Pollution in an Agricultural Watershed, China. *Sci. Total Environ.* **2022**, *823*, 153680. [CrossRef]

41. Minet, E.P.; Goodhue, R.; Meier-Augenstein, W.; Kalin, R.M.; Fenton, O.; Richards, K.G.; Coxon, C.E. Combining Stable Isotopes with Contamination Indicators: A Method for Improved Investigation of Nitrate Sources and Dynamics in Aquifers with Mixed Nitrogen Inputs. *Water Res.* **2017**, *124*, 85–96. [CrossRef]
42. Li, S.; Jiang, H.; Guo, W.; Zhang, W.; Zhang, Q. From Soil to River: Revealing the Mechanisms Underlying the High Riverine Nitrate Levels in a Forest Dominated Catchment. *Water Res.* **2023**, *241*, 120155. [CrossRef]
43. Gao, Z.; Su, J.; Ali, A.; Wang, X.; Bai, Y.; Wang, Y.; Wang, Z. Denitrification Strategy of Pantoea Sp. MFG10 Coupled with Microbial Dissimilatory Manganese Reduction: Deciphering the Physiological Response Based on Extracellular Secretion. *Bioresour. Technol.* **2022**, *355*, 127278. [CrossRef]
44. Labbé, N.; Parent, S.; Villemur, R. Addition of Trace Metals Increases Denitrification Rate in Closed Marine Systems. *Water Res.* **2003**, *37*, 914–920. [CrossRef]
45. Liu, C.-Q.; Li, S.-L.; Lang, Y.-C.; Xiao, H.-Y. Using Δ15N- and Δ18O-Values To Identify Nitrate Sources in Karst Ground Water, Guiyang, Southwest China. *Environ. Sci. Technol.* **2006**, *40*, 6928–6933. [CrossRef]
46. Panno, S.V.; Hackley, K.C.; Hwang, H.H.; Greenberg, S.E.; Krapac, I.G.; Landsberger, S.; O'Kelly, D.J. Characterization and Identification of Na-Cl Sources in Ground Water. *Groundwater* **2006**, *44*, 176–187. [CrossRef] [PubMed]
47. Wang, W.; Song, X.; Ma, Y. Identification of Nitrate Source Using Isotopic and Geochemical Data in the Lower Reaches of the Yellow River Irrigation District (China). *Environ. Earth Sci.* **2016**, *75*, 936. [CrossRef]
48. Gómez-Alday, J.J.; Hussein, S.; Arman, H.; Alshamsi, D.; Murad, A.; Elhaj, K.; Aldahan, A. A Multi-Isotopic Evaluation of Groundwater in a Rapidly Developing Area and Implications for Water Management in Hyper-Arid Regions. *Sci. Total Environ.* **2022**, *805*, 150245. [CrossRef] [PubMed]
49. Elagouz, M.H.; Abou-Shleel, S.M.; Belal, A.A.; El-Mohandes, M.A.O. Detection of Land Use/Cover Change in Egyptian Nile Delta Using Remote Sensing. *Egypt. J. Remote Sens. Space Sci.* **2020**, *23*, 57–62. [CrossRef]
50. Eissa, M.; Ali, M.; Zaghlool, E.; Stash, O.S. Hydrochemical and Stable Isotopes Indicators for Detecting Sources of Groundwater Contamination Close to Bahr El-Baqar Drain, Eastern Nile Delta, Egypt. *Water Sci.* **2019**, *33*, 54–64. [CrossRef]
51. Hussien, R.; Ahmed, M.; Aly, A.I. Tracking Anthropogenic Nitrogen-Compound Sources of Surface and Groundwater in Southwestern Nile Delta: Hydrochemical, Environmental Isotopes, and Modeling Approach. *Environ. Sci. Pollut. Res.* **2023**, *30*, 22115–22136. [CrossRef]
52. CAPMAS. Arab. Republic of Egypt—General. Census for Population, Housing and Establishments. 2017. Available online: https://censusinfo.capmas.gov.eg/metadata-en-v4.2/index.php/catalog/621 (accessed on 17 December 2023).
53. *RIGW-IWACO Hydrogeological Map of Egypt, 1:2000,000*; Research Institute of Groundwater, Water Research Center, Ministry of Public Works and Water Resources, Arab Republic of Egypt: Cairo, Egypt, 1992.
54. Hefny, K.; Khalil, J.B. General Hydrogeological Condition of Greater Cairo Area. *Water Sci. J Oct.* **1989**, *6*, 13–19.
55. Khalil, M.M.; Tokunaga, T.; Yousef, A.F. Insights from Stable Isotopes and Hydrochemistry to the Quaternary Groundwater System, South of the Ismailia Canal, Egypt. *J. Hydrol.* **2015**, *527*, 555–564. [CrossRef]
56. Awad, M.A.; El Arabi, N.E.; Hamza, M.S. Use of Solute Chemistry and Isotopes to Identify Sources of Ground-Water Recharge in the Nile Aquifer System, Upper Egypt. *Groundwater* **1997**, *35*, 223–228. [CrossRef]
57. Abu Salem, H.; Gemail, K.S.; Nosair, A.M. A Multidisciplinary Approach for Delineating Wastewater Flow Paths in Shallow Groundwater Aquifers: A Case Study in the Southeastern Part of the Nile Delta, Egypt. *J. Contam. Hydrol.* **2021**, *236*, 103701. [CrossRef]
58. American Public Health Association. *Standard Methods for the Examination of Water and Wastewater*, 23rd ed.; Rice, E.W., Bridgewater, L., American Public Health Association, Eds.; American Public Health Association: Washington, DC, USA, 2017.
59. Sigman, D.M.; Casciotti, K.L.; Andreani, M.; Barford, C.; Galanter, M.; Böhlke, J.K. A Bacterial Method for the Nitrogen Isotopic Analysis of Nitrate in Seawater and Freshwater. *Anal. Chem.* **2001**, *73*, 4145–4153. [CrossRef] [PubMed]
60. Weigand, M.A.; Foriel, J.; Barnett, B.; Oleynik, S.; Sigman, D.M. Updates to Instrumentation and Protocols for Isotopic Analysis of Nitrate by the Denitrifier Method. *Rapid Commun. Mass. Spectrom.* **2016**, *30*, 1365–1383. [CrossRef] [PubMed]
61. El-Fakharany, M.A.; Mansour, N.M.; Yehia, M.M.; Monem, M. Evaluation of Groundwater Quality of the Quaternary Aquifer through Multivariate Statistical Techniques at the Southeastern Part of the Nile Delta, Egypt. *Sustain. Water Resour. Manag.* **2017**, *3*, 71–81. [CrossRef]
62. Hegazy, D.; Abotalib, A.Z.; El-Bastaweesy, M.; El-Said, M.A.; Melegy, A.; Garamoon, H. Geo-Environmental Impacts of Hydrogeological Setting and Anthropogenic Activities on Water Quality in the Quaternary Aquifer Southeast of the Nile Delta, Egypt. *J. Afr. Earth Sci.* **2020**, *172*, 103947. [CrossRef]
63. Craig, H. Isotopic Variations in Meteoric Waters. *Science* **1961**, *133*, 1702–1703. [CrossRef] [PubMed]
64. Han, R.; Liu, W.; Zhang, J.; Zhao, T.; Sun, H.; Xu, Z. Hydrogeochemical Characteristics and Recharge Sources Identification Based on Isotopic Tracing of Alpine Rivers in the Tibetan Plateau. *Environ. Res.* **2023**, *229*, 115981. [CrossRef]
65. Awad, M.A.; Hamza, M.S.; Farid, M.S. Studies on the Recharge of the Aquifer Systems in the Southern Portion of the Nile Delta Using Radioisotopes and Hydro Chemistry. *Isot. Radiat. Res.* **1994**, *26*, 17.
66. Hamza, M.S.; Aly, A.I.M.; Swailem, F.M.; Nada, A. Environmentally Stable Isotopes and Groundwater Recharge in the Eastern Nile Delta. *Int. J. Water Resour. Dev.* **1987**, *3*, 228–232. [CrossRef]
67. Zhang, W.; Jiang, H.; Guo, W.; Li, S.; Zhang, Q. Unexpectedly High Nitrate Levels in a Pristine Forest River on the Southeastern Qinghai-Tibet Plateau. *J. Hazard. Mater.* **2023**, *458*, 132047. [CrossRef]

68. Widory, D.; Petelet-Giraud, E.; Négrel, P.; Ladouche, B. Tracking the Sources of Nitrate in Groundwater Using Coupled Nitrogen and Boron Isotopes: A Synthesis. *Environ. Sci. Technol.* **2005**, *39*, 539–548. [CrossRef]
69. Jin, J.; Wang, Z.; Zhao, Y.; Ding, H.; Zhang, J. Delineation of Hydrochemical Characteristics and Tracing Nitrate Contamination of Groundwater Based on Hydrochemical Methods and Isotope Techniques in the Northern Huangqihai Basin, China. *Water* **2022**, *14*, 3168. [CrossRef]
70. Torres-Martínez, J.A.; Mora, A.; Mahlknecht, J.; Daesslé, L.W.; Cervantes-Avilés, P.A.; Ledesma-Ruiz, R. Estimation of Nitrate Pollution Sources and Transformations in Groundwater of an Intensive Livestock-Agricultural Area (Comarca Lagunera), Combining Major Ions, Stable Isotopes and MixSIAR Model. *Environ. Pollut.* **2021**, *269*, 115445. [CrossRef] [PubMed]
71. Spoelstra, J.; Leal, K.A.; Senger, N.D.; Schiff, S.L.; Post, R. Isotopic Characterization of Sulfate in a Shallow Aquifer Impacted by Agricultural Fertilizer. *Groundwater* **2021**, *59*, 658–670. [CrossRef] [PubMed]
72. Torres-Martínez, J.A.; Mora, A.; Knappett, P.S.K.; Ornelas-Soto, N.; Mahlknecht, J. Tracking Nitrate and Sulfate Sources in Groundwater of an Urbanized Valley Using a Multi-Tracer Approach Combined with a Bayesian Isotope Mixing Model. *Water Res.* **2020**, 115962. [CrossRef] [PubMed]
73. Papazotos, P.; Vasileiou, E.; Perraki, M. The Synergistic Role of Agricultural Activities in Groundwater Quality in Ultramafic Environments: The Case of the Psachna Basin, Central Euboea, Greece. *Environ. Monit. Assess.* **2019**, *191*, 317. [CrossRef] [PubMed]
74. Ahmed, M.A.; Abdel Samie, S.G.; Badawy, H.A. Factors Controlling Mechanisms of Groundwater Salinization and Hydrogeochemical Processes in the Quaternary Aquifer of the Eastern Nile Delta, Egypt. *Environ. Earth Sci.* **2013**, *68*, 369–394. [CrossRef]
75. Rashed, M.; Awad, S.R.; Salam, M.A.; Smidt, E. Monitoring of Groundwater in Gabal El Asfar Wastewater Irrigated Area (Greater Cairo). *Water Sci. Technol.* **1995**, *32*, 163–169. [CrossRef]
76. Al-Gamal, S.; El-Sayed, S.; Atta, E. Exploring Surface-and Groundwater Interactions in East Delta Aquifer Using Conventional and Nonconventional Techniques. *J. Appl. Geol. Geophys.* **2018**, *6*, 48–58.
77. Jørgensen, P.R.; Urup, J.; Helstrup, T.; Jensen, M.B.; Eiland, F.; Vinther, F.P. Transport and Reduction of Nitrate in Clayey till underneath Forest and Arable Land. *J. Contam. Hydrol.* **2004**, *73*, 207–226. [CrossRef]
78. Desireddy, S.; Pothanamkandathil Chacko, S. A Review on Metal Oxide (FeOx/MnOx) Mediated Nitrogen Removal Processes and Its Application in Wastewater Treatment. *Rev. Environ. Sci. Biotechnol.* **2021**, *20*, 697–728. [CrossRef]
79. Gerardi, M.H. Nitrogen: Environmental and Wastewater Concerns. In *Nitrification and Denitrification in the Activated Sludge Process*; John Wiley & Sons, Inc.: Hoboken, NJ, USA, 2002; pp. 1–9.
80. Barzegar, R.; Moghaddam, A.A.; Tziritis, E.; Fakhri, M.S.; Soltani, S. Identification of Hydrogeochemical Processes and Pollution Sources of Groundwater Resources in the Marand Plain, Northwest of Iran. *Environ. Earth Sci.* **2017**, *76*, 297. [CrossRef]
81. Zhao, M.; Jiang, Y.; Jia, Y.; Lian, X.; Feng, F.; Shang, C.; Zang, Y.; Xi, B. Anthropogenic Perturbation Enhances the Release of Geogenic Mn to Groundwater: Evidence from Hydrogeochemical Characteristics. *Sci. Total Environ.* **2023**, *891*, 164450. [CrossRef]
82. Ji, X.; Shu, L.; Chen, W.; Chen, Z.; Shang, X.; Yang, Y.; Dahlgren, R.A.; Zhang, M. Nitrate Pollution Source Apportionment, Uncertainty and Sensitivity Analysis across a Rural-Urban River Network Based on Δ15N/Δ18O-NO_3^- Isotopes and SIAR Modeling. *J. Hazard. Mater.* **2022**, *438*, 129480. [CrossRef]
83. Kendall, C.; McDonnell, J.J. *Isotope Tracers in Catchment Hydrology*; Elsevier: Amsterdam, The Netherlands, 1998; ISBN 008092915X.
84. Wankel, S.D.; Kendall, C.; Francis, C.A.; Paytan, A. Nitrogen Sources and Cycling in the San Francisco Bay Estuary: A Nitrate Dual Isotopic Composition Approach. *Limnol. Oceanogr.* **2006**, *51*, 1654–1664. [CrossRef]
85. Rivett, M.O.; Buss, S.R.; Morgan, P.; Smith, J.W.N.; Bemment, C.D. Nitrate Attenuation in Groundwater: A Review of Biogeochemical Controlling Processes. *Water Res.* **2008**, *42*, 4215–4232. [CrossRef] [PubMed]
86. Jiang, H.; Liu, W.; Li, Y.; Zhang, J.; Xu, Z. Multiple Isotopes Reveal a Hydrology Dominated Control on the Nitrogen Cycling in the Nujiang River Basin, the Last Undammed Large River Basin on the Tibetan Plateau. *Environ. Sci. Technol.* **2022**, *56*, 4610–4619. [CrossRef] [PubMed]
87. Michener, R.; Lajtha, K. (Eds.) *Stable Isotopes in Ecology and Environmental Science*; Blackwell Publishing Ltd.: Oxford, UK, 2007; ISBN 9780470691854.
88. Homoncik, S.C.; MacDonald, A.M.; Heal, K.V.; Ó Dochartaigh, B.É.; Ngwenya, B.T. Manganese Concentrations in Scottish Groundwater. *Sci. Total Environ.* **2010**, *408*, 2467–2473. [CrossRef] [PubMed]
89. Yoch, D.C. Manganese, an Essential Trace Element for N_2 Fixation by *Rhodospirillum rubrum* and *Rhodopseudomonas capsulata*: Role in Nitrogenase Regulation. *J. Bacteriol.* **1979**, *140*, 987–995. [CrossRef]
90. Bennett, P.C.; El Shishtawy, A.M.; Sharp, J.M.; Atwia, M.G. Source and Migration of Dissolved Manganese in the Central Nile Delta Aquifer, Egypt. *J. Afr. Earth Sci.* **2014**, *96*, 8–20. [CrossRef]
91. Hou, Q.; Zhang, Q.; Huang, G.; Liu, C.; Zhang, Y. Elevated Manganese Concentrations in Shallow Groundwater of Various Aquifers in a Rapidly Urbanized Delta, South China. *Sci. Total Environ.* **2020**, *701*, 134777. [CrossRef]
92. Salem, M.G.; El-Awady, M.H.; Amin, E. Enhanced Removal of Dissolved Iron and Manganese from Nonconventional Water Resources in Delta District, Egypt. *Energy Procedia* **2012**, *18*, 983–993. [CrossRef]
93. Hamimi, Z.; El-Barkooky, A.; Martínez Frías, J.; Fritz, H.; Abd El-Rahman, Y. (Eds.) *The Geology of Egypt*, 1st ed.; Springer International Publishing: Cham, Switzerland, 2020; ISBN 978-3-030-15264-2.

94. EEBS. Geological, Hydrological and Geomorphological Properties of Soil for Egyptian Governorates. In *Soil Atlas of Egypt*; Part Egyptian Education Building Society Publication: Cairo, Egypt, 2004; pp. 1–290.
95. Egyptian Geological Survey. *Geologic Map of Egypt, Scale 1:2,000,000*; Egyptian Geological Survey and Mining Authority: Cairo, Egypt, 1981.
96. Karra, K.; Kontgis, C.; Statman-Weil, Z.; Mazzariello, J.C.; Mathis, M.; Brumby, S.P. Global Land Use/Land Cover with Sentinel 2 and Deep Learning. In Proceedings of the 2021 IEEE International Geoscience and Remote Sensing Symposium IGARSS, Brussels, Belgium, 11–16 July 2021; pp. 4704–4707.